PONTIFICIA UNIVERSIDAD CATOLICA DE CHILE
ESCUELA DE INGENIERIA

MATHEMATICAL SIMULATION OF HEAT AND MASS TRANSFER DURING CONTROLLED DEPRESSURIZATION OF SUPERCRITICAL CO_2 IN EXTRACTION VESSELS

MARÍA SOLEDAD MURIAS PALOMER

Thesis submitted to the Office of Research and Graduate Studies in partial fulfillment of the requirements for the Degree of Master of Science in Engineering

Advisor:
JOSÉ MANUEL DEL VALLE

Santiago de Chile, (April, 2016)

PONTIFICIA UNIVERSIDAD CATOLICA DE CHILE
ESCUELA DE INGENIERIA

MATHEMATICAL SIMULATION OF HEAT AND MASS TRANSFER DURING CONTROLLED DEPRESSURIZATION OF SUPERCRITICAL CO_2 IN EXTRACTION VESSELS

MARÍA SOLEDAD MURIAS PALOMER

Members of the Committee:

JOSÉ MANUEL DEL VALLE L.

CLAUDIO GELMI W.

GONZALO NÚÑEZ M.

JOSÉ FRANCISCO MUÑOZ P.

Thesis submitted to the Office of Research and Graduate Studies in partial fulfillment of the requirements for the Degree of Master of Science in Engineering

Santiago de Chile, (April, 2016)

(To my parents, brothers, friends, and teachers for their unwavering support.)

ACKNOWLEDGMENTS

This research was funded by Fondecyt projects 1120827 and 1150623. I would like to thank Chilean agency Conicyt for a scholarship to carry out MSc. studies in Engineering Science in UC (CONICYT-PCHA/Magíster Nacional/2015 - folio 22151040). I would also like to thank Simula UC for lending me a computer powerful enough to run the simulations, and Prof. Claudio Gelmi, for his insight on Matlab and heat transfer.

GENERAL INDEX

TABLE INDEX

FIGURE INDEX

RESUMEN

Aun con casi cuarenta años presente en la industria, las compañías son reacias a utilizar CO_2 supercrítico (sc) como solvente en extracciones debido a que piensan que los costos de producción serán elevados. La literatura en este tema sugiere que utilizar múltiples extractores simulando flujo contracorriente podría abaratar los costos de producción. Sin embargo, a más extractores se usen, menos tiempo habrá para reacondicionarlos si se desea tener una operación semi-continua; y si la despresurización se realiza demasiado rápido, el material del extractor puede dañarse permanentemente. Pensando en una eventual optimización de este proceso, se realizó un modelo que simula las variaciones de temperatura y masa de un extractor de 1 L cargado con materiales. Se utilizaron correlaciones reportadas en literatura para calcular el flujo de masa, conductividades efectivas y convección entre el sólido y el fluido. Mediante optimización, se obtuvieron parámetros de una correlación para el coeficiente de transferencia de calor en la pared del extractor, resultando en la ecuación $Nu = 0.0777\ Da^{-0.0373}\ Ra^{0.397}$. Las simulaciones para temperatura, presión y flujo de masa evacuada fueron razonablemente buenas, además de que se mejoraron los valores predichos en un 20% con respecto a los obtenidos usando una correlación propuesta en la literatura. Para explorar el uso del modelo en situaciones prácticas, se simularon despresurizaciones con diferentes volúmenes de extractor, geometrías del mismo, y condiciones iniciales. Las pruebas con extractores de hasta 1 m^3 mostraron que era posible usar el volumen para obtener la apertura de válvula que permite mantener la temperatura mínima por sobre cierta temperatura. Las pruebas con diferentes condiciones iniciales en extractores de 1 m^3 mostraron que los cambios de estado en el CO_2 eran relevantes a la hora de determinar el efecto de la temperatura inicial sobre la despresurización. El máximo tiempo de despresurización obtenido fue de 54.5 minutos en un extractor de 1 m^3 comenzando a 60 °C y 70 MPa. Este modelo puede ser usado más adelante para determinar el tiempo de reacondicionamiento óptimo para plantas industriales en una minimización de costos.

ABSTRACT

Even after almost forty years of industrial application, companies are still reluctant to use supercritical (sc) CO_2 as a solvent for extractions due to the perceived high production costs. Literature on the matter suggests that using multiple extraction vessels simulating countercurrent flow could reduce operational costs. However, as the number of extraction vessels increases, the time available for recondition them decreases in order to have a semi-continuous operation; and when the depressurization is done too fast, the vessel be damaged permanently. With the goal of optimizing this process in mind, numerical simulation of temperature and mass was carried considering a 1-L vessel filled with an exhausted packed bed made with model materials. Literature correlations were used for mass flow, effective conductivity and solid-to-fluid convection. The parameters for a correlation for the convective heat transfer coefficient at the vessel wall were optimized resulting in the equation $Nu = 0.0777\ Da^{-0.0373}\ Ra^{0.397}$. Temperature, pressure, and vented mass flow were simulated and predictions improved in almost 20% in comparison with simulations with our previous correlation. To explore the use of the model for practical purposes, it was used to simulate depressurizations with different vessel volumes and geometries, and initial conditions. Tests for a 1-m^3 vessel showed that it was possible to use the volume to obtain the valve opening needed to keep the minimum temperature above a chosen temperature. Tests with different initial conditions for a 1-m^3 vessel showed that phase changes within the CO_2 were determinant in order to assess the effect of initial temperature over depressurizations. Simulated depressurization times reached a maximum value of 54.5 minutes for depressurizations of a 1-m^3 extraction vessel starting at 60 °C and 70 MPa, which are very plausible extraction conditions. This model can be later used to determine optimal reconditioning time in industrial plants for cost minimization.

Key words: carbon dioxide; depressurization; heat transfer; mathematical simulation; packed bed.

1. INTRODUCTION

Extraction processes have multiple uses in today's industries for both removing undesirable compounds and for obtaining a pure sample of desirable ones. Now more than ever, interest in obtaining active compounds or beneficial substances from natural sources has been growing (Herrero, Cifuentes, & Ibañez, 2006), which makes the necessity of obtaining pure, uncontaminated products even more relevant. Organic solvents such as acetone (Garcia-Viguera, Zafrilla, & Tomás-Barberán, 1998), water (Mustafa & Turner, 2011), hexane and butane (Reverchon & De Marco, 2006) have been used for extracting organic matrices and, to enhance their properties, some of them have been used in their supercritical state.

Supercritical (sc) fluid extraction (SFE) refers to the extraction of compounds using a solvent in its supercritical state. A fluid is in a supercritical state when its temperature and pressure are above the fluid critical point, as shown in Figure 1. Some of the benefits of using supercritical fluids are that the solubility can be easily modified by small changes in pressure or temperature and that its high diffusivity makes for a faster extraction as the solvent easily enters the organic matrix (Reverchon & De Marco, 2006). Among the solvents used for SFE, carbon dioxide (CO_2) stands out and has become very popular due to its many advantages over the other solvents. First, CO_2 is not harmful and it leaves no traces in the final product because it is naturally a gas at atmospheric conditions. Also, the critical point of CO_2 (30.98 °C and 73.8 bar) is suitable for thermolabile compounds and it is easily reachable in comparison with other sc fluids like water (critical point: 373.9 °C and 22.1 bar) or hexane (critical point: 234.5 °C and 30.2 bar). Finally, CO_2 is a relatively economic solvent and it can be recycled into the extraction vessel without contributing to the environmental CO_2 (Brunner, 2005).

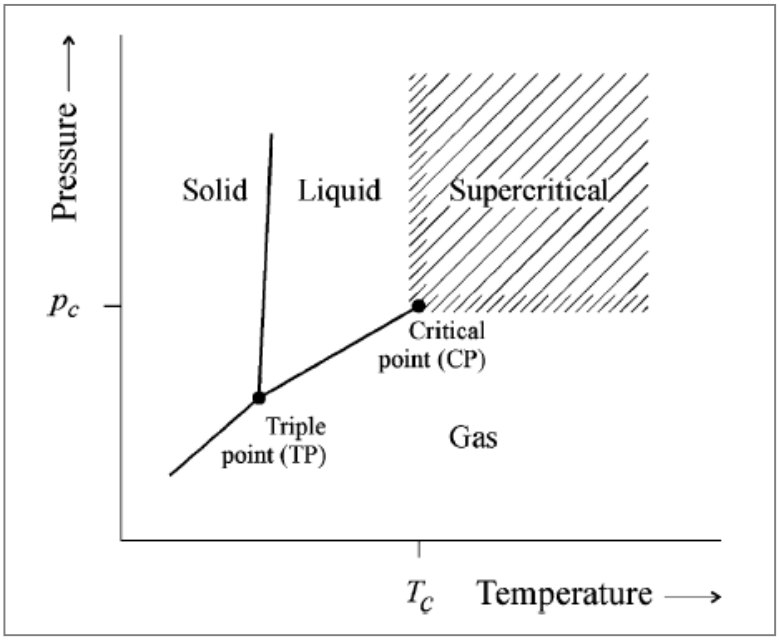

Figure 1. Definition of supercritical state for a pure fluid (Brunner, 2005).

Even though $scCO_2$ has many advantages over other organic solvents and has been used as an extraction solvent for almost four decades, companies still hesitate when it comes to investing in this technology (del Valle, 2015). The reasons for these doubts may be the perceived high costs associated with operating an extraction plant. However, cost optimization could prove to be the tool needed in order to refute such beliefs.

Núñez and del Valle (2014) optimized production costs in a $scCO_2$ extraction plant. Some of the relevant variables for minimization were mass flow rate (inversely proportional to production costs; production costs decreased when increasing mass flow rate), aspect ratio of the extraction vessel (directly proportional to production costs for a constant superficial velocity of CO_2), and number of extraction vessels working in parallel (inversely proportional to production costs).

SFEs using $scCO_2$ operate in batch processes due to the high pressures requires and, when using extraction vessels connected in series, it is desired to have all the extraction vessels working in a semi-continuous manner, as depicted in Figure 2. This means that

the vessel where an extraction just finished needs to be reconditioned in the time it takes the next packed bed to become exhausted (Fiori, 2010). One limiting aspect of increasing the number of extraction vessels is the reduction of available reconditioning time. In other words, reconditioning time for semi-continuous operation needs to be on the (*n* -1)-th part of the total extraction time (where *n* is the number of extraction vessels used), which makes reconditioning time inversely proportional to the number of extraction vessels.

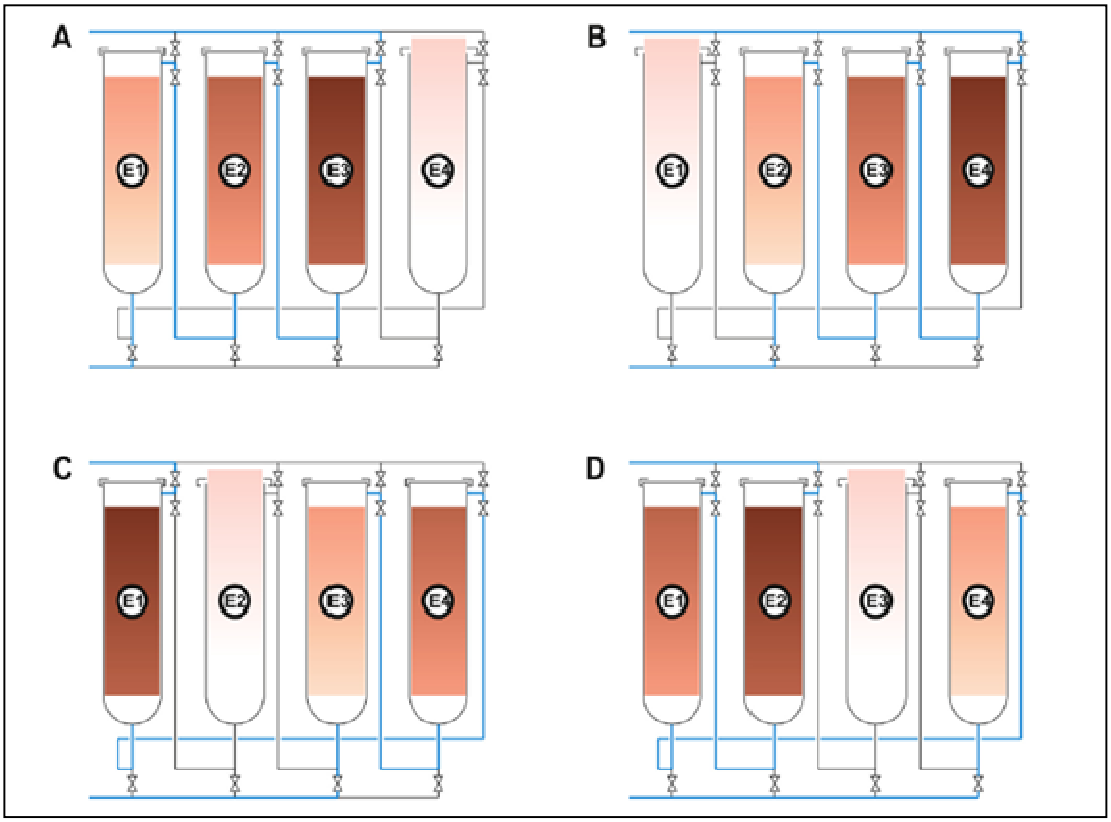

Figure 2. Schematic representation of a four-vessel supercritical fluid extraction plant operating in parallel (the color represents the freshness of the material; the darker the color, the fresher the material) where one of the extraction vessels is in reconditioning process while the other three are carrying out extractions at different progress (del Valle, 2015). As the sequence progress, the reconditioned extraction vessel takes the place of the most exhausted one. Blue lines represent the solvent cycle.

The reconditioning process consists of four steps: (i) depressurization of the vessel, (ii) unloading of the exhausted material, (iii) loading of fresh material, and (iv) pressurization of the vessel. The second and third steps are limited by the plant capacity and of the personnel carrying out the process, and the last one is limited by the power of the pump used for that purpose. This leaves the depressurization process as the one with greater possibilities for study and optimization. The focus of previous research has been mostly on safety aspects (Eggers & Green, 1990; Gebbeken & Eggers, 1996; Zhang *et al.*, 2014) but not on the practical aspects of it.

Setting the speed of depressurization is not as simple as opening the valve as far as it goes. Not only does temperature drops when pressure descends, but due to the Joule-Thompson effect in adiabatic depressurizations (Stanley, 1998), temperature can drop as far as the sublimation temperature for CO_2, which would thus change into dry ice. This is a problem because the materials that make up the extraction vessel have minimum conditions (including temperature) at which to work under or else they could become brittle (Smallman & Ngan, 2007) and permanently damaged.

For the reasons explained previously, it is necessary to find the conditions that would allow depressurizations to occur fast enough to allow for semi-continuous operation in the industries, but that would guaranty the safety of the equipment used and of the people manipulating it. No formulae have been proposed in this aspect in the literature, and only in the last few years has experimental research been done on the subject.

2. HYPOTHESIS AND OBJECTIVES

The hypothesis of this work is that the controlled depressurization of an extraction vessel can be simulated in order to estimate and optimize the depressurization time.

The aim of this work was to develop a mathematical model that accurately simulated heat and mass transfer during the controlled depressurization of an extraction vessel filled with CO_2 and a packed bed made from a model material. From this general objective follow the specific objectives:

1. To assess existing literature in order to determine the equations that would best fit the process and its restrictions.
2. To determine the parameters for a new correlation for Nusselt number (in order to estimate the heat transfer coefficient in the vessel wall) in function on dimensionless numbers Rayleigh and Darcy.
3. To validate the developed mathematical model by comparing experimental data with simulations.
4. To explore the use of the model for practical purposes by running simulations in vessels with different volumes, geometries and starting at different initial conditions.

This thesis is divided in 7 Chapters: Chapters 1 and 2 presented the introduction and objectives of this thesis respectively, Chapter 3 is a literature survey about heat transfer in a packed bed and previous work on simulations involving situations similar to the one of interest in this thesis, Chapter 4 describes the material and methods used in this work, and Chapters 5 and 6 describe the results and discussion, respectively. Chapter 7 summarizes the conclusions of this thesis and proposes future work on this subject.

3. LITERATURE SURVEY

This Chapter will be divided into two subsections. Subsection 3.1 presents the literature survey about heat transfer in a packed bed and some of the correlations that have been proposed to explain the phenomena occurring. Subsection 3.2 exposes some of the research that have been done on depressurizations.

3.1 Heat transfer in a packed bed

Three subjects relating heat transfer in packed beds will be presented in this subsection. The first one will be effective thermal conductivities, which are correcting factors for thermal conductivities in order to take into account the setup in which the materials are put. The second subject will be on how to calculate the heat transfer coefficient between the solid and the fluid phase in a packed bed. The last subject will be a review of the research involving how to calculate the heat transfer coefficient between the vessel wall and the packed bed and fluid.

3.1.1 Effective conductivities in a packed bed

Effective conductivities have been studied as early as 1934, when Schumann & Voss (1934) proposed a correlation for heat flow in a granulated material. Since then, several correlations for effective axial and radial conduction for both solid and fluid phases have been proposed but it was only in 1960 that effective conductivities were proposed specifically for packed beds. In that year, Yagi *et al.* (1960) measured effective thermal conductivities in a reactor with a packed bed and determined that the axial conductivity could not be neglected, as it had been done previously. They determined that the axial and radial effective thermal conductivity could be calculated by the sum of the thermal conductivity in a motionless fluid (k_0^{eff}) and the product between the thermal conductivity of the fluid (k_f), the Péclet number, and a constant δ, which had different values depending on the case (radial or axial conductivity), as seen in Eq. (1). Proposed

values for the constant were between 0.1 and 0.3 for radial thermal conductivity, and between 0.7 and 0.8 for axial thermal conductivity.

$$k_{\text{eff}} = k_0^{\text{eff}} + \delta \cdot k_{\text{f}} \cdot Pe \tag{1}$$

The thermal conductivity in a static fluid was calculated using the porosity, the thermal conductivity of the fluid and of the material packed, and two factors that depend on the "density" of the packaging (how loose or close are the particles to each other) (Eq. 2).

$$k_0^{\text{eff}} = \varepsilon + (1-\varepsilon) \cdot \left(\frac{C_{\text{y}}}{\gamma + \frac{2k_{\text{f}}}{3k_{\text{s}}}} \right) \tag{2}$$

Following studies focused on how to calculate the static thermal conductivity (Kunii & Smith, 1960; Schlünder, 1966) until 1970, when Zehner and Schlünder (1970) presented a model for a one-dimensional effective thermal conductivity, but failed to consider conduction through pellets with large surface contact area. Vortmeyer & Scheafer (1974) modified the model proposed by Yagi *et al.* by changing the second term in order to make the equation suitable for different materials (Eq. 3).

$$k_{\text{eff}} = k_0^{\text{eff}} + \frac{k_{\text{f}} \cdot Pe^2}{6 \cdot (1-\varepsilon) \cdot Bi} \tag{3}$$

Later on, Dixon and Creswell (1979) proposed models for both axial (Eq. 4a) and radial (Eq. 4b) effective conductivities for a pseudo-homogeneous model which incorporated for the first time the fluid-to-solid heat transfer coefficient as a relevant term.

$$\left(k_{\text{f}}^{\text{eff}}\right)_{\text{r}} = 1 + \frac{k_{\text{s}}}{k_{\text{f}}} \left(\frac{(1-\varepsilon)\left(\frac{2R}{d_{\text{p}}}\right)^2 \left(1 + \frac{8k_{\text{f}}}{2RU}\right)}{1 + \frac{16}{3} k_{\text{s}} \left(\frac{1}{h_{\text{fs}} d_{\text{p}}} + \frac{0.1}{k_{\text{s}}} \right)} \right), \text{ and} \tag{4a}$$

$$\left(k_{\mathrm{f}}^{\mathrm{eff}}\right)_{\mathrm{z}} = 1 + \frac{k_{\mathrm{s}}}{k_{\mathrm{f}}} \left(\frac{(1-\varepsilon)^2 \left(\frac{2R}{d_{\mathrm{p}}}\right)^4}{\left(1 + \frac{16}{3} k_{\mathrm{s}} \left(\frac{1}{h_{\mathrm{fs}} d_{\mathrm{p}}} + \frac{0.1}{k_{\mathrm{s}}} \right)\right)^2} \right) \tag{4b}$$

Wakao & Kaguei (1982) included the correlations proposed by Yagi *et al.* in their book but gave their constants values of 0.1 and 0.5 for radial and axial conductivity respectively. A new proposition was made by Winterberg & Tsotsas (2000) for axial effective thermal conductivity, neglecting among other factors the radial thermal conductivity (Eq. 5).

$$k_{\mathrm{eff}} = k_0^{\mathrm{eff}} + 0.5 \cdot Pe \cdot k_{\mathrm{f}} \tag{5}$$

In recent years, Younis (2006) included the effect of radiation in the effective thermal conductivity term (Eq. 6) but later on, Nield & Bejan (2006) work suggested that not only it was not necessary to include this term but also that effective thermal conductivity could be calculated as the weighted arithmetic mean (Eq. 7a) or the weighted geometric mean (Eq. 7b) of the thermal conductivities.

$$k_{\mathrm{eff}} = \left[\varepsilon \cdot k_{\mathrm{f}} + (1-\varepsilon) \cdot \left(k_{\mathrm{s}} + \frac{16 \cdot \sigma \cdot T^3}{3 \cdot \beta} \right) \right] \tag{6}$$

$$k_{\mathrm{eff}} = \varepsilon \cdot k_{\mathrm{f}} + (1-\varepsilon) \cdot k_{\mathrm{s}} \tag{7a}$$

$$k_{\mathrm{eff}} = k_{\mathrm{f}}^{\varepsilon} \cdot k_{\mathrm{s}}^{(1-\varepsilon)} \tag{7b}$$

3.1.2 Fluid-to-solid heat transfer

The study of the heat transfer coefficient between the solid and the fluid phase of a packed bed dates back to 1943, when Gamson *et al.* (1943) proposed correlations depending on the flow regimen (Eq. 8). Simplifying the previous contribution, Hanz

(1952) proposed that it could be calculated using only the Reynolds and Prandtl numbers (Eq. 9). This equation had a good fit with experimental data in turbulent flow range, but failed to predict values for laminar flows.

$$h_{\mathrm{fs}} = \begin{cases} 1.064 \cdot c_{\mathrm{p}} \cdot F \cdot \rho^{-1} \cdot Re^{-2/3} \cdot Pr^{-0.41} & \mathrm{Re} \geq 350 \\ 18.1 \cdot c_{\mathrm{p}} \cdot F \cdot \rho^{-1} \cdot Re^{-2/3} \cdot Pr^{-1} & \mathrm{Re} \leq 40 \end{cases} \tag{8}$$

$$Nu_{\mathrm{fs}} = 2 + 0.6 \cdot Re^{1/3} \cdot Pr^{1/2} \tag{9}$$

Initially, this problem was attributed to very different causes. Kunii & Suzuki (1967) claimed that the reason was flow channeling in the bed, while Nelson & Galloway (1975) argued that it was because of the renewal of the fluid surrounding each particle, and Martin (1978) pointed out that the non-uniformity of the packing could be responsible for these discrepancies. Schlünder (1978) even showed under what assumptions the Nusselt number could decrease continuously with the Reynolds number.

This issue is still being debated, with two clear different views being predominant. While some say that the Nusselt number decreases continuously as the Reynolds number does so, others say that it only decreases until it reaches a limiting Nusselt number at zero flow rate (Wakao & Kaguei, 1982). Values for the limiting Nusselt number varied from 3.8 to 18 (Gunn, 1978; Miyauchi, 1971; Pfeffer & Happel, 1964; Schlünder, 1975; Sørensen & Stewart, 1974) until Wakao *et al.* (1978) showed that the problem was in the fundamental equation used and proposed new parameters for the typical equation (Eq. 10) taking into account most of the experimental results up to date (Figure 3)

$$Nu_{\mathrm{fs}} = 2 + 1.1 \cdot Pr^{1/3} \cdot Re^{0.6} \tag{10}$$

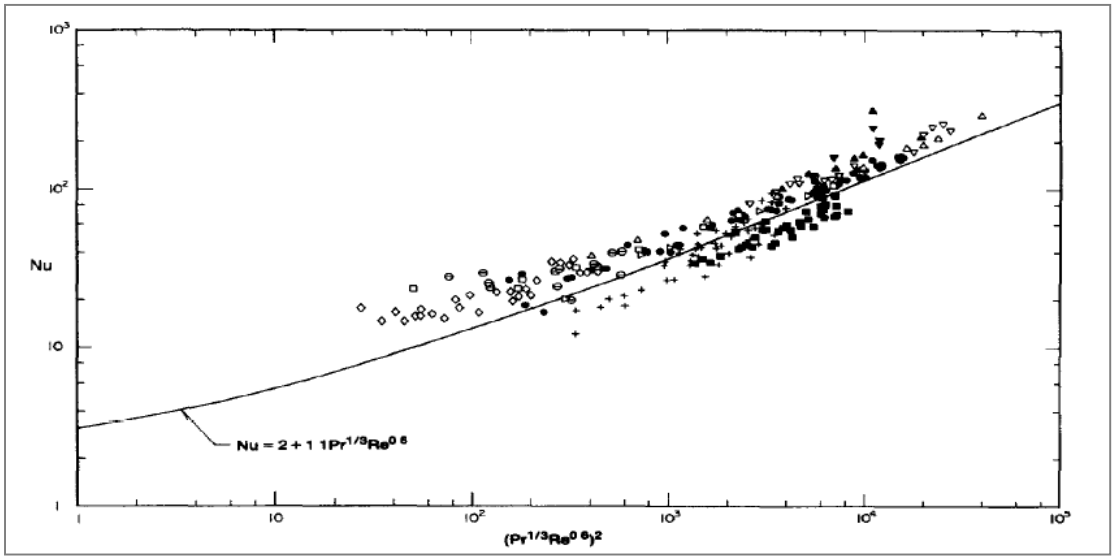

Figure 3. Correlation for particle-to-solid Nusselt number adapter from Wakao *et al.* (1978).

3.1.3 Wall heat transfer

Heat transfer coefficient from the wall to the packed bed has been typically determined by mass transfer experiments and heat and mass transfer analogies. Yagi & Wakao (1959) estimated this coefficient by measuring the dissolution rate of a coated material in direct contact with the wall and then making heat and mass transfer analogies (Eq. 11). The validity of this equation in the Reynolds lower region is doubtful because they fail to take into account axial dispersion in their analysis.

$$Nu_w = \begin{cases} 0.6 \cdot Pr^{1/3} \cdot Re^{1/2} & 1 \le Re \le 40 \\ 0.2 \cdot Pr^{1/3} \cdot Re^{0.8} & 40 \le Re \le 2000 \end{cases} \tag{11}$$

Taking this into account, Olbrich & Potter (1972) measured the vaporization of mercury from the wall into a nitrogen stream and proposed a new correlation for heat transfer (Eq. 12). Their results are significantly different from those obtained by Yagi & Wakao because they had to account for multiple phenomena in their calculations, including pressure drop and axial dispersion.

$$Nu_w = 8.9 \cdot Pr^{1/3} \cdot Re^{0.34} \quad 100 \leq Re \leq 3000 \tag{12}$$

Dixon & Creswell (1979) later proposed a correlation for the Biot number (Eq. 13), instead of the Nusselt number, that depended exclusively on the Reynolds number (and not Prandtl). However, this correlation could be only validated for Reynolds numbers higher than 40.

$$Bi \cdot \left(\frac{d_p}{R} \right) = 3 \cdot Re^{-0.25} \tag{13}$$

Because of the failure of most previous correlations to predict wall heat transfer coefficients in the lower Reynolds region and particularly for depressurizations, Richter *et al.* (2015) proposed an experimental design which allowed them to calculate the heat being transferred from the vessel wall and lids and propose a correlation for heat transfer that depended on the Rayleigh (*Ra*) dimensionless number. They later improved their experimental setup and proposed a correlation using *Ra* and the Darcy (*Da*) dimensionless number in order for it to be suitable for multiple packed beds and different vessel geometries (Eq. 14). It was not possible to find other literature correlations that depended on *Ra* and *Da*.

$$Nu_w = 0.086 \cdot Ra^{0.357} \cdot Da^{-0.037} \tag{14}$$

3.2 Previous work on depressurizations

The depressurization of a vessel filled with either only a fluid or a fluid and a packed bed has not been extensively studied. Most studies have centered on safety issues and did not relate the changes observed to properties of the substrate or the fluid. Only recently experimental data was used to relate the physical changes in the CO_2 to the different stages commonly defined for a depressurization process.

At the start of the 90s, Eggers & Green (1990) made experimental observations about temperature and pressure changes in depressurizations. Their study focused on the formation of dry ice and the conditions needed to avoid it. They conclude that if the

liquid phase of CO_2 fills less than 20% of the vessel volume, then temperature would not fall below -10 °C. Their depressurizations were made with valve opening areas ranging from 5.6 to 56 mm^2.

Following that study, Gebbeken & Eggers (1996) designed an experimental setup which allowed them to measure temperature at several points in the vessel and study axial thermal profiles. They studied the effect of valve opening area and initial pressure and temperature (Figure 4), and observed phase transition by means of a gamma densitometer in a 50 L vessel filled only with CO_2. Their results indicated that initial temperature affected initial drop in pressure, which was steeper with lower temperatures, but later pressures tended to converge to the same point and then follow similar progress. Similar results were obtained at different starting pressures, where pressure drop was more abrupt with higher initial pressures. The authors attribute this to higher initial specific entropy. On the contrary, valve opening did not appear to affect pressure drop until after saturation. Axial profiles did not appear until after phase separation, which was to be expected.

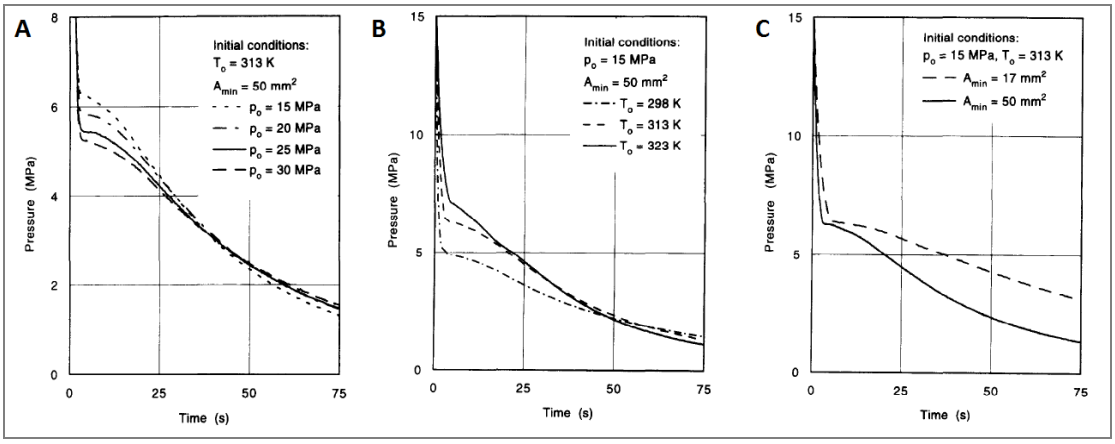

Figure 4. Effect of initial pressure (A), initial temperature (B), and valve opening (C) in pressure drop through depressurization of a 50 L vessel filled with pure subcooled liquid or supercritical CO_2 adapted from Gebbeken & Eggers (1996).

Zhang *et al.* (2014) studied depressurizations and searched for a model to be used to define safety margins for operation. They propose three different models in order to

account for the different stages found in Gebbeken & Eggers work. These models were the homogeneous mixture model, the complete separation model, and the bubble rising model. The first one is used to neglect the phase separation effect; the second, neglects immersed bubbles in the liquid phase; and the last one considers phase separation with submerged bubbles in the liquid phase. They used the experimental results obtained by Gebbeken & Eggers to compare to the results of their models (Figure 5) but results were not very satisfactory in all three cases. Phase separation appears to have an effect in pressure drop in the middle stages of the depressurization but not on the initial and final stages of it.

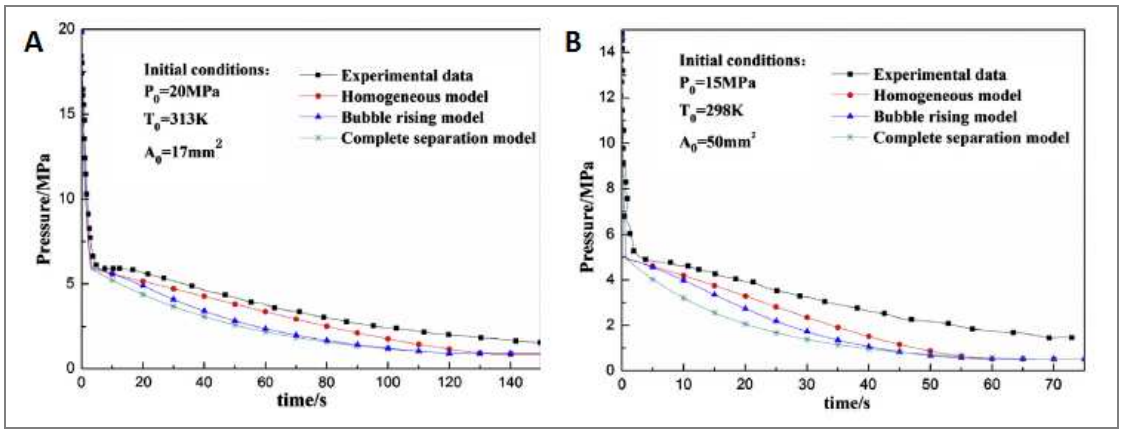

Figure 5. Comparison made by Zhang *et al.* (2014) between the models they proposed and experimental results obtained by Gebbeken & Eggers (1996).

As mentioned previously, Richter *et al.* (2015) studied depressurization with the future goal of being able to optimize this process for the industry in mind. They packed four different exhausted materials (pressed or pelletized raspberry and rosehip) into a one gallon reactor which had four thermocouples connected in different places and proceeded to vent the CO_2 using a valve opening small enough so that no phase separation occurred. They also did this using the same vessel filled only with CO_2. Their results showed that the initial drop in pressure stopped when CO_2 crossed the pseudocritical line (i.e., the limit at sc conditions that differentiate gas-like and liquid-

like fluids that corresponds to a local maxima in specific heat) and that depressurization time was proportional to packed bed porosity. They correlated vented mass flow to chocked flux and a constant identified as the valve opening area. Also, using calculated energy balances, they propose a correlation for heat transfer from the vessel wall.

As part of their conclusions, Richter *et al.* (2015) suggest that the use of model materials (geometry and physical properties known) would be beneficial because the physical properties of the ones used were too similar to make relevant comments of the effect of the properties of the packed bed over depressurization. Because of this, Richter *et al.* (submitted) conducted a similar experiment using a 1 L extraction vessel (detailed in Figure 6) and three different model material (sintered steel cylinders, glass beads and Raschig rings). The properties of these materials can be found in Table 1.

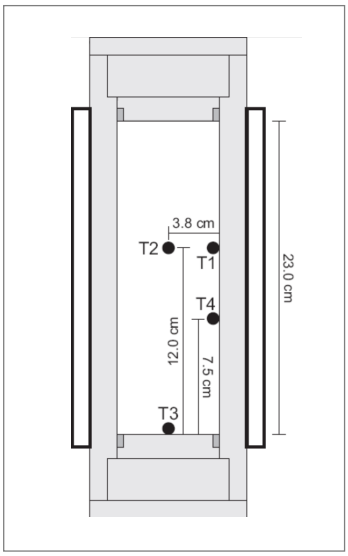

Figure 6. Geometry of the vessel and thermocouples positions used for experiments performed by Richter *et al.* (submitted).

The results of this work were the validation of results obtained in similar experiments (Richter *et al.*, 2015) and a new correlation for heat transfer coefficient through the vessel wall (Eq. 14). This correlation was better than the one proposed before because it included *Da* as a parameter. This allowed for one equation for different materials instead of one for each.

Table 1. Characterization of the material packed in the experiments performed by Richter *et al.* (submitted).

Physical property	Sintered stainless steel	Glass beads	Glass Raschig rings
Shape	Solid cylinder	Sphere	Hollow cylinder
Diameter (mm)	7.9	3	8.3
Height (mm)	8	-	8.3
Internal diameter (mm)	-	-	5.9
Solid density (kg m^{-3})	7740	2490	2370
Particle density (kg m^{-3})	5980	2490	-
Bulk density (kg m^{-3})	2960	1330	600
Intraparticle porosity (–)	0.25	0.00	0.19
Interparticle porosity (–)	0.51	0.47	0.69
Total porosity (–)	0.62	0.47	0.75
Solid thermal conductivity (W m^{-1} K^{-1})	9.4	1.2	1.2
Specific heat (kJ kg^{-1} K^{-1})	0.502	0.84	0.84
Darcy number (-)	7.77×10^{-7}	2.02×10^{-9}	1.27×10^{-5}

Although an improvement from previous work, the experimental design proposed by Richter *et al.* (submitted) had some deficiencies. It is possible that the number of thermocouples placed in the vessel was insufficient to stablish the existence of axial or

radial temperature profiles throughout the depressurization vessel. Also, it is difficult to measure the temperature of the fluid near the vessel wall; mass flow could have caused vibrations or movement in the thermocouple placed in there that could have in turn affected measurements.

As exposed by this literature survey, there has been no successful modelling of the depressurization process and the ones proposed until now have been sorely focused on the safety aspect. Therefore, there is an opportunity to further optimize an industrial process by improving the productivity of a $scCO_2$ extraction plant, which could make it more attractive to investors and in turn provide people with accessible high-quality products.

4. MATERIALS AND METHODS

This section is divided in three parts. The first one shows the assumptions and considerations made in order to simplify the model. The second part shows the equations used to model heat and mass transfer in the extraction vessel. Finally, we describe the numerical method used, how error and confidence intervals were calculated, and how we tested the effect of some operational parameters on depressurization processes.

4.1 Model assumptions

In order to produce a model for controlled CO_2 depressurization, several assumptions had to be made. First, differences in pressure within the extraction vessel were considered negligible. Physical properties of the packed bed (bulk density and porosity) and of the steel wall (thermal conductivity and heat capacity) were assumed to be constant during depressurization because of the small changes in them in the temperature interval between 250 and 350 K. The thermal diffusivity of steel was obtained from Bergman *et al.* (2011).

Experimental results obtained by Richter *et al.* (submitted) were used to validate the results obtained through simulation. These experiments were carried out in a 1 dm^3 extraction vessel with a heating jacket and with experimental conditions shown in Table 2. The vessel was loaded with a packed bed made from three possible model materials: sintered stainless steel cylinders, glass beads, and glass Raschig rings. Experimental depressurizations with packed beds were carried out in two stages depending on the valve opening. Initially, the valve opening was small (flow coefficient f_c = 0.0005; flow coefficient is a measure of the efficiency of the valve in letting fluid flow) to avoid phase separation due to experimental restrictions. Valve opening was increased (f_c = 0.0086) when mass flow was no longer detectable by the flow meter. The geometry and dimensions of the extraction vessel and the packed material used in the experimental design can be found in Figure 3 and Table 1.

Table 2. Operation conditions used for simulation.

Temperature of heating water (°C)	60
Initial temperature (°C)	60
Initial pressure (MPa)	26
Radium of extraction vessel (mm)	38
Thickness of extraction vessel wall (mm)	18.5
Height of extraction vessel (mm)	230
Volume of extraction vessel (m^3)	0.001

4.2 Mass and heat transfer in the system

A single vessel filled with CO_2 at high pressure and temperature and a packed bed made from model materials was considered. Also, the solid temperature was calculated separately from that of the fluid. The equations that represent the mass and energy balances along the vessel were adapted from the ones used by Slimi *et al.* (1997). The mass balance is given by Eq. (15).

$$\frac{dm}{dt} = -F(t), \tag{15}$$

where $F(t) = A\rho\upsilon$, and $F(t)$ is the product between the chocked mass flux at the exit of the nozzle (calculated as the product between the fluid density ρ and the speed of sound υ) and the area of the opening of the valve (A), as suggested by Richter *et al.* (2015). The values of A were obtained experimentally.

The components of the energy balances for the fluid (Eq. 16a) and the solid (Eq. 16b) are energy loss due to fluid motion, heat conduction within the solid phase, heat convection within the fluid phase expressed as effective conductivity, heat convection between solid and fluid phases, and energy loss due to mass being evacuated.

$$\frac{\partial T_f}{\partial t} = -\frac{u}{\varepsilon}\frac{\partial T_f}{\partial z} + \frac{\alpha_f}{\varepsilon}\left[\left(k_f^{eff}\right)_r \frac{1}{r}\frac{\partial}{\partial r}\left(r\frac{\partial T_f}{\partial r}\right) + \left(k_f^{eff}\right)_z \frac{\partial^2 T_f}{\partial z^2} - \frac{h_{fs}\alpha_{fs}}{k_f}\left(T_f - T_s\right) - \frac{F(t)h}{2\pi rRLk_f}\right] \tag{16a}$$

$$\frac{\partial T_s}{\partial t} = \frac{\alpha_s}{1-\varepsilon}\left[k_s^{\text{eff}} \left(\frac{\partial^2 T_s}{\partial r^2} + \frac{1}{r}\frac{\partial T_s}{\partial r} + \frac{\partial^2 T_s}{\partial z^2} \right) + \frac{1}{k_s} h_{fs} \alpha_{fs} \left(T_f - T_s \right) \right] \tag{16b}$$

Energy balance for the vessel wall was calculated using the same equations used in Richter *et al.* (submitted). Bulk porosity was calculated using the correlations proposed by Dixon (1988) for spheres (Eq. 17a) and cylinders (Eq. 17b).

$$\varepsilon = \begin{cases} 0.4 + 0.05\dfrac{d_p}{2R} + 0.412\left(\dfrac{d_p}{2R}\right)^2, & \dfrac{d_p}{2R} \le 0.5, \\ 0.528 + 2.464\left(\dfrac{d_p}{2R} - 0.5\right), & 0.5 \le \dfrac{d_p}{2R} \le 0.536, \text{ and} \\ 1 - 0.667\left(\dfrac{d_p}{2R}\right)^3 \left(\dfrac{d_p}{R} - 1\right)^{-0.5}, & 0.536 \le \dfrac{d_p}{2R}, \end{cases} \tag{17a}$$

$$\varepsilon = \begin{cases} 0.36 + 0.1\dfrac{d_p}{2R} + 0.7\left(\dfrac{d_p}{2R}\right)^2, & \dfrac{d_p}{2R} \le 0.6, \\ 0.677 - 9\left(\dfrac{d_p}{2R} - 0.625\right)^2, & 0.6 \le \dfrac{d_p}{2R} \le 0.7, \text{ and} \\ 1 - 0.763\left(\dfrac{d_p}{2R}\right)^2, & 0.7 \le \dfrac{d_p}{2R}. \end{cases} \tag{17b}$$

The fluid-to-solid heat transfer (h_{fs}) coefficient was based on an empirical correlation proposed by Wakao *et al.* (1978) (Eq. 18) and the solid-fluid exchange area (α_{fs}) was calculated using Eq. (19).

$$h_{fs} = \frac{k_f}{d_p}\left[2 + 1.1\left(Pr_f^{1/3} Re_f^{0.6} \right) \right], \tag{18}$$

$$\alpha_{fs} = \frac{6(1-\varepsilon)}{d_p} \text{ for spheres, and} \tag{19a}$$

$$\alpha_{fs} = \frac{4 \cdot (d + l) \cdot (1-\varepsilon)}{d \cdot l} \text{ for cylinders,} \tag{19b}$$

where *d* and *l* are the diameter and height of the packed cylinder, respectively.

Effective thermal conductivities for the fluid and solid phase were calculated using the correlations proposed by Dixon and Creswell (1979) that are shown in Eq. (20).

$$\left(k_{\mathrm{f}}^{\mathrm{eff}}\right)_{\mathrm{r}} = 1 + \frac{k_{\mathrm{s}}}{k_{\mathrm{f}}}\left(\frac{(1-\varepsilon)\left(\frac{2R}{d_{\mathrm{p}}}\right)^{2}\left(1+\frac{8k_{\mathrm{f}}}{2Rh_{\mathrm{w}}}\right)}{1+\frac{16}{3}k_{\mathrm{s}}\left(\frac{1}{h_{\mathrm{fs}}d_{\mathrm{p}}}+\frac{0.1}{k_{\mathrm{s}}}\right)}\right), \tag{20a}$$

$$\left(k_{\mathrm{f}}^{\mathrm{eff}}\right)_{\mathrm{z}} = 1 + \frac{k_{\mathrm{s}}}{k_{\mathrm{f}}}\left(\frac{(1-\varepsilon)^{2}\left(\frac{2R}{d_{\mathrm{p}}}\right)^{4}}{\left(1+\frac{16}{3}k_{\mathrm{s}}\left(\frac{1}{h_{\mathrm{fs}}d_{\mathrm{p}}}+\frac{0.1}{k_{\mathrm{s}}}\right)\right)^{2}}\right), \text{ and} \tag{20b}$$

$$k_{\mathrm{s}}^{\mathrm{eff}} = (1-\varepsilon). \tag{20c}$$

The initial and boundary conditions used to solve the mathematical model are shown in Eq. (21) and Eq. (22), respectively. Initial conditions are not chosen arbitrarily but given by the extraction conditions; the depressurization starts just after the extraction ends, so the extraction temperature and pressure are the starting temperature and pressure of the depressurization.

$$T_{\mathrm{f}}\big|_{t=0} = T_{\mathrm{s}}\big|_{t=0} = T_{\mathrm{J}}\ ,\ t=0 \tag{21}$$

$$T_{\mathrm{f}}\big|_{r=R} = \frac{h_{\mathrm{w}}}{\left(h_{\mathrm{w}}+k_{\mathrm{w}}/x_{\mathrm{w}}\right)}T_{\mathrm{f}}\big|_{r=0}\ \forall\ \mathrm{z},\ \mathrm{t}, \tag{22a}$$

$$k_{\mathrm{s}}\left.\frac{\partial T_{\mathrm{s}}}{\partial r}\right|_{r=R} = k_{\mathrm{w}}\left.\frac{\partial T_{\mathrm{w}}}{\partial r}\right|_{r=R}\ \forall\ \mathrm{z},\ \mathrm{t}, \tag{22b}$$

$$\left.\frac{\partial T_{\mathrm{f}}}{\partial r}\right|_{r=0} = \left.\frac{\partial T_{\mathrm{s}}}{\partial r}\right|_{r=0} = 0\ \forall\ \mathrm{z},\ \mathrm{t}, \tag{22c}$$

$$T_{\mathrm{f}}\big|_{r=0} = \left(\frac{h_{\mathrm{w}}}{h_{\mathrm{w}} + k_{\mathrm{w}} / x_{\mathrm{l}}} \right) T_{\mathrm{f}}\big|_{\substack{r=0 \\ z=h/2}} \quad \forall \text{ t and } z = \{0, L\} \text{ , and} \tag{22d}$$

$$T_{\mathrm{s}}\big|_{r=0} = \left(\frac{h_{\mathrm{w}}}{h_{\mathrm{w}} + k_{\mathrm{w}} / x_{\mathrm{l}}} \right) T_{\mathrm{s}}\big|_{\substack{r=0 \\ z=h/2}} \quad \forall \text{ t and } z = \{0, L\} \text{ ,} \tag{22e}$$

where h_w is the heat transfer coefficient between the steel wall and the fluid, calculated using a correlation like the one proposed by Richter *et al.* (submitted), shown in Eq. (23). The parameters of this correlation were obtained by minimizing the least square error between the experimental and simulated data.

$$h_{\mathrm{w}} = \frac{k_{\mathrm{f}}}{L} \left(a \, Da^{b} \, Ra^{\mathrm{c}} \right) \tag{23}$$

The dimensionless Rayleigh (*Ra*), and Darcy (*Da*) numbers were calculated as proposed by Richter *et al.* (submitted) with the height of the vessel *L* as the characteristic length, using the following equations:

$$Ra = \frac{g\beta \left(T_{\mathrm{w}} - \bar{T} \right) L^{3}}{\nu\alpha} \text{ , and} \tag{24a}$$

$$Da = \frac{\kappa}{L^{2}} \tag{24b}$$

where α, β, and ν are the thermal diffusivity, volumetric thermal expansion coefficient, and kinematic viscosity of the CO_2, respectively, and κ is the permeability of the packed bed, which we calculated using the equation of Carman-Kozeny (Schlünder & Tsotsas, 1988), Eq. (25):

$$\kappa = \frac{d_{\mathrm{p}}^{2} \varepsilon_{\mathrm{e}}^{3}}{150 \left(1 - \varepsilon_{\mathrm{e}} \right)^{2}} \text{ ,} \tag{25}$$

where d_p is the particle size or equivalent diameter and ε_e is the interparticle porosity

4.3 Numerical method, parameter optimization, and sensibility

Both solid and fluid phases were divided in 10 nodes in the radial direction and 10 nodes in the axial direction. This number was chosen because it was the smallest at which adding one more node made no difference in the results. The resulting equations were 201 in total: i) one hundred differential equations to account for the heat transfer in the fluid; ii) one hundred differential equation to represent the heat transfer in the solid phase of the packed bed; iii) one equation to represent the mass transfer between the system and the surroundings. Central finite differences where used for the spatial derivatives as discretization method. The resulting time-dependent system was resolved using the ode23s solver in MATLAB R2012a (MathWorks, Natick, MA). Parameter optimization was carried out in the same software using the *nlinfit* function and confidence intervals were obtained with the *nlparci* function. This last function calculates the 95% confidence interval of optimized parameters using their value, residual value, and Jacobian matrix, all of which are given by the *nlinfit* function. The complete code can be seen in Appendices A-E.

For optimization, only the results of sintered steel cylinders and glass beads were used. This was so, because a Raschig ring is not a commonly used shape of packed bed materials in the industry, unlike cylinders or spheres. In order to measure the difference between the simulated and experimental results, a Mean Absolute Percentage Error (*MAPE*) was calculated using Eq. (26).

$$MAPE = \frac{1}{n}\sum_{i=1}^{n}\frac{|y_i - f(x_i)|}{y_i} \tag{26}$$

System pressure was calculated in each iteration using mean temperature and density (calculated dividing the total CO_2 mass in the vessel by the effective volume) into the state equation proposed by Huang *et al.* (1984). Physical properties, such as ρ and c_p, of pure CO_2 were obtained using the NIST Database (Lemmon, Huber, & McLinden, 2007) with local temperature and system pressure as inputs. All of these properties were updated in every iteration of the ode solver by introducing the updated local temperature

and system pressure into the NIST function for MATLAB, *refpropm*. In the event of phase separation, the NIST database needs the user to specify if the properties given are those of a gas or a liquid. Because of this, physical properties when phase separation occurs where calculated as the weighted mean between their values in the liquid and gas state and the weight was the quality of the mixture.

To explore the use of the model for practical purposes, we simulated different depressurization processes with varying parameters, like vessel volume and geometry, and initial pressure and temperature. We tested five different vessel volumes filled with CO_2 and a packed bed made of 1 cm glass beads following a progression from laboratory scale, to pilot scale, and to industrial scale. Tested volumes were 0.005 m^3, 0.08 m^3, 0.25 m^3, 0.5 m^3 and 1 m^3 with an aspect ratio equal to 5 (*i.e.* the height-to-diameter ratio meaning that, for an aspect ratio of 5, if the vessel has a diameter of 1 m then its height will be 5 m) chosen by the authors based on a similar assumption made by Núñez *et al*. (2011). Valve opening for each case was chosen so that the minimum temperature in the system did not decrease below 0 °C as a precaution so that the vessel material does not become brittle (Smallman & Ngan, 2007). Four different aspect ratios (4, 4.5, 5, and 6) were also tested in a 1-m^3 vessel using the same valve opening found in the previous step. The same was done with different initial temperature and pressure, where tested values were 60, 70, and 80 °C at 30 MPa, and 30, 50, and 70 MPa at 60 °C, respectively. These values were chosen because they are plausible temperatures of the thermal fluid in the heating jacket and extraction pressures, respectively.

All of these simulations were run until the pressure inside the vessel reached near-atmospheric values. The thickness of the steel wall and lids in these tests were calculated using standard formulae in literature for pressurized vessel design (Bednat, 1996). The geometry of the vessels for each test can be found on Appendix F. The number of nodes was not increased for these tests due to the lack of experimental results to compare the simulations with, so we chose to keep the time needed to run each test to a minimum in order to be able to test the effect of additional parameters.

5. RESULTS

The new optimized equation for convective heat transfer at the vessel wall is shown in Eq. (27). Confidence intervals for all nine parameters can be found in Table 3. Adjustment between simulated and experimental temperatures improved by 18% when using these new parameters; the mean absolute percentage error decreased from 8.1% to 6.6% (Figure 7). Figure 8 shows simulated temperatures (Fig. 8A), pressures (Fig. 8B), and mass venting rate (Fig. 8C) using Eq. (27) Adjustment is also satisfactory for pressure drop and for mass venting rate.

$$Nu = 0.0777\ Da^{-0.0373}\ Ra^{0.397} \tag{27}$$

Table 3. Parameters and confidence intervals for the regression $Nu = a\ Da^{b}\ Ra^{c}$ between Nusselt dimensionless number (*Nu*), and Rayleigh (*Ra*) and Darcy (*Da*) dimensionless numbers.

Parameter	Lower value	Estimated value	Upper value
a	0.0772	0.0777	0.0783
b	-0.0374	-0.0373	-0.0372
c	0.3940	0.3967	0.3990

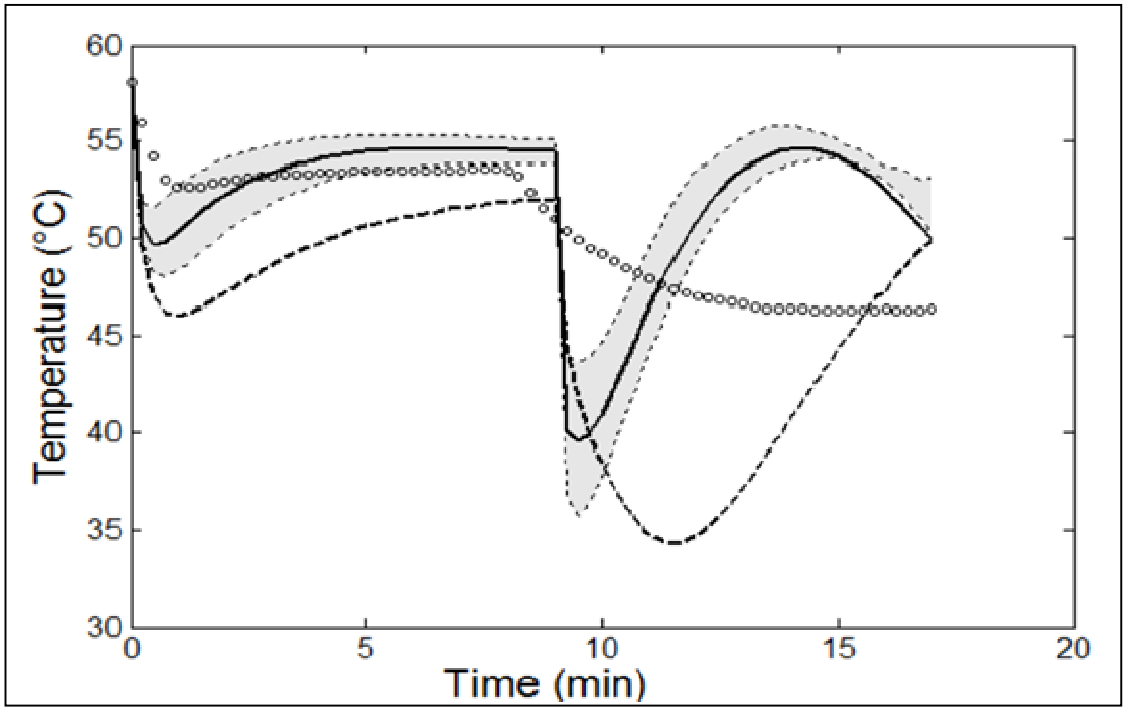

Figure 7. Comparison between simulated temperatures using Eq. (14) for heat transfer through the wall (——), simulated temperatures using our previous correlation (Richter *et al.*, submitted) for heat transfer through the wall (-------), and experimental results (Richter *et al.*, submitted) (○) for depressurizations starting at 60 ºC and 26 MPa packed with sintered steel cylinders. The greyed area is delimited by results using the optimized parameter with a ±10% variation

Figure 9 shows the simulated temperatures for all points of the extraction vessel at the start of the process (1 min), after increasing the valve opening, and at the middle of the depressurization (12 min). Although temperature changes throughout the process, the distribution of the temperature along the vessel does not drastically change. This is not the case with the temperature distribution in the solid (Fig. 9A-C).

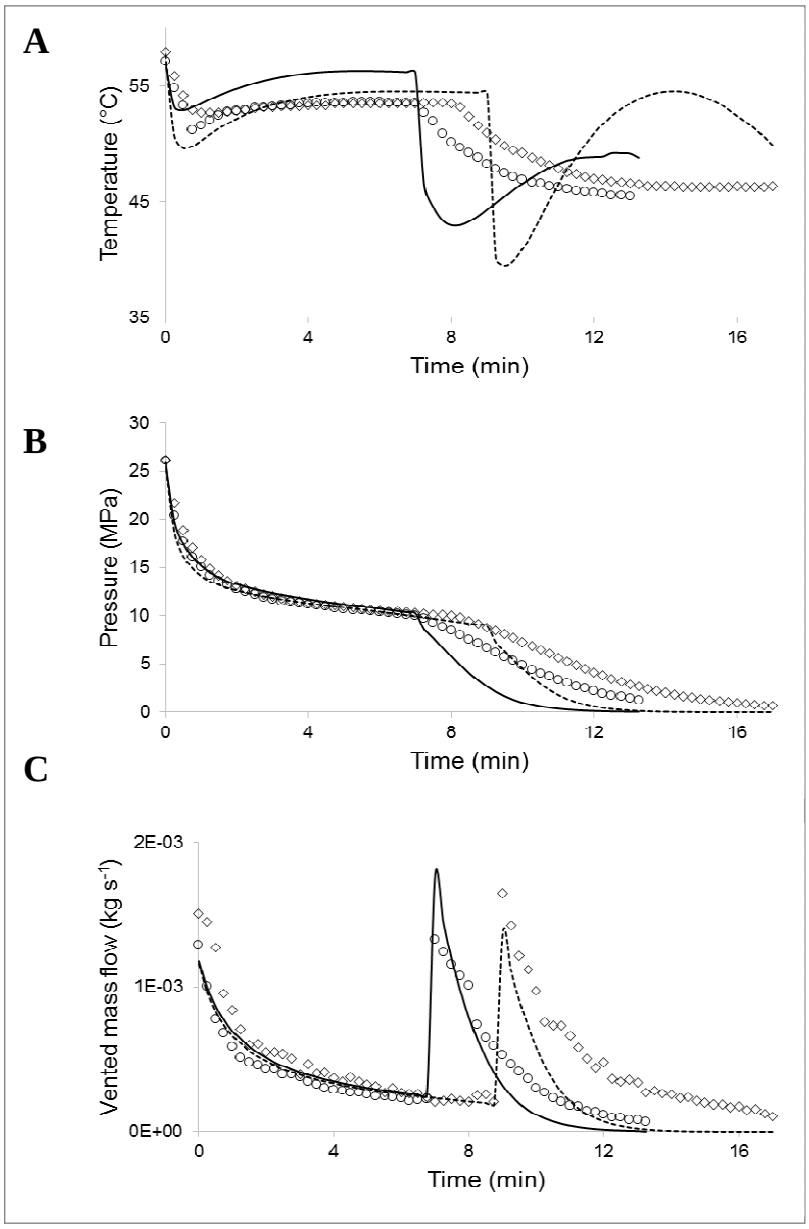

Figure 8. Comparison between simulated temperature (A), pressure (B) and mass venting rate (C), and experimental results (Richter *et al.*, submitted) for depressurizations starting at 60 ºC and 26 MPa packed with sintered steel cylinders (-------- , ◊), and glass beads (——— , ○).

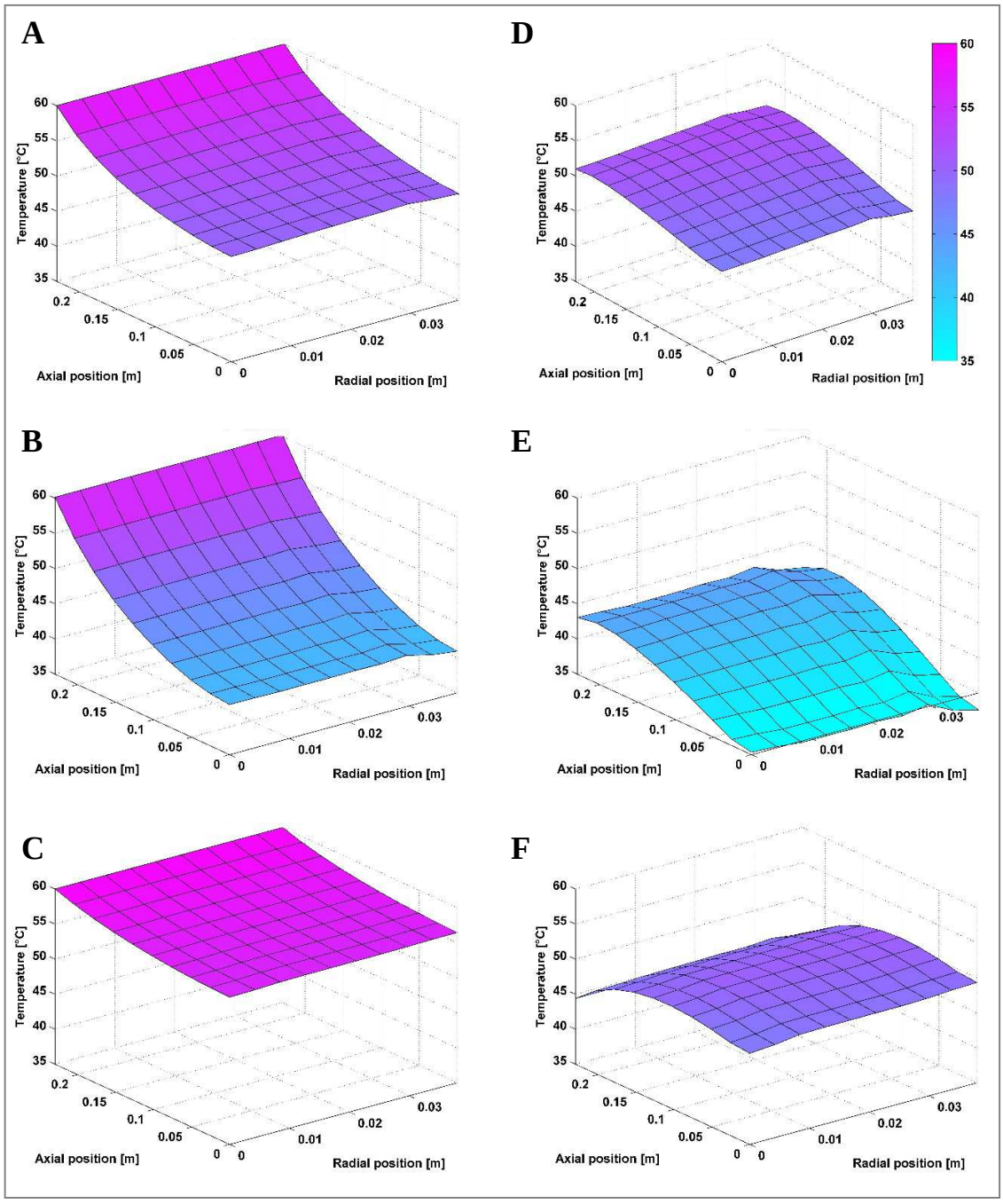

Figure 9. Simulated solid (A-C) and fluid (D-F) temperatures in the vessel for depressurizations with sintered steel cylinders starting at 60 °C and 30 MPa after 1 minute (A, D), after increasing the valve opening (B, E), and after 12 minutes of starting the process (C, F).

Simulations with different vessel volume and geometry, and initial pressure and temperature were run until the vessel pressure neared atmospheric values. However, in practical applications it is preferable to stop before this point as the time needed to decrease 1 MPa rises considerably after saturation conditions are met. Because of this, Table 4 shows the time needed for the vessel to reach 1 MPa for all tests. Note that this time is an overestimation of the actual depressurization time in an industrial plant, because it is not practical to work with a constant valve opening area. In practical applications, workers will further open the valve if dry ice is not observed. As referential values, Fiori (2010) suggests that the total time for reconditioning should be around one hour for optimal operation and Quirin & Gerard (2007) estimate it to be around 45 to 90 minutes. These last authors also state that the depressurization process is the most time-consuming.

Figure 10 shows results of tests with different volumes. Simulation of a 0.5-m^3 extraction vessel are not shown because they were virtually the same as simulations for a 1-m^3 vessel. Total depressurization times went from 8 to 19 minutes. The valve opening used in each case was chosen so that temperature reached 0 °C at the lowest. These openings are shown as a function on vessel volume in Figure 11. The correlation $\log(A) = 1.04\log(V) - 4.81$ was found between valve opening chosen and vessel volume with a R^2 coefficient of 0.97.

Table 4. Summary table for simulated time required for an extraction vessel to decrease its pressure to 1 MPa at different vessel geometries, starting conditions, and constant valve opening area.

Vessel volume (L)	Aspect ratio (L/D)	Initial temperature (°C)	Initial pressure (MPa)	Valve opening area (mm^2)	Time to reach 1 MPa (min)
5	5.0	60	30	0.08	5.00
80	5.0	60	30	0.60	11.17
250	5.0	60	30	5.00	11.67
500	5.0	60	30	11.00	13.50
1000	4.0	60	30	16.00	13.83
1000	4.5	60	30	16.00	13.16
1000	5.0	60	30	16.00	12.83
1000	6.0	60	30	16.00	10.83
1000	5.0	60	50	16.00	26.83
1000	5.0	60	70	16.00	54.50
1000	5.0	70	30	16.00	3.83
1000	5.0	80	30	16.00	7.33

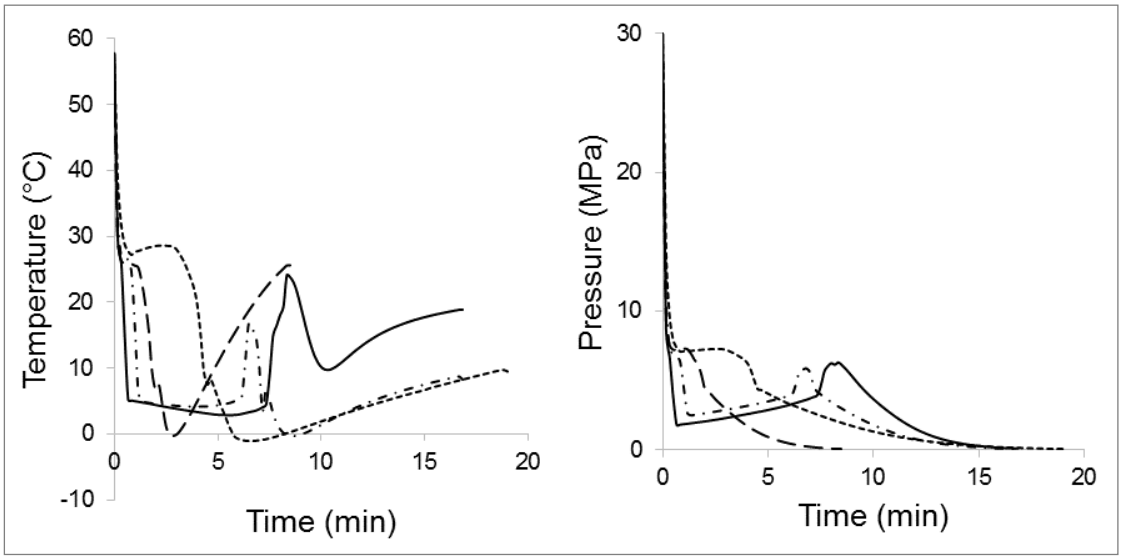

Figure 10. Temperature and pressure changes for depressurizations starting at 60 °C and 30 MPa with different vessel volumes (– – V = 0.005 m^3; ------- V = 0.08 m^3; – · – · V = 0.25 m^3; ——— V = 1 m^3) packed with glass beads.

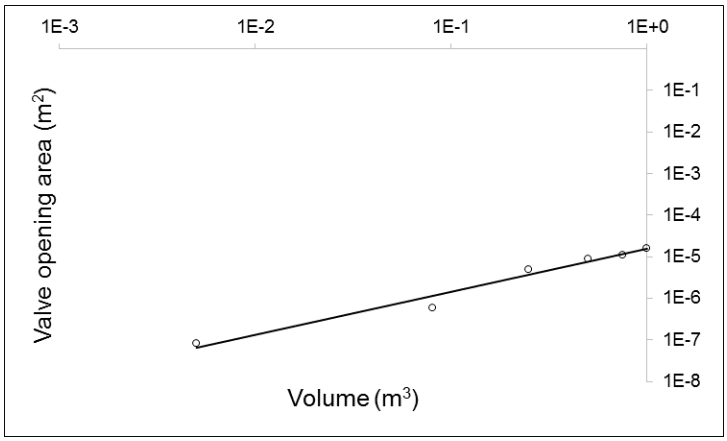

Figure 11. Valve opening area required for minimum temperature not to decrease below 0 °C (symbols) in depressurizations starting at 60 °C and 30 MPa, and correlation of that opening as a function of vessel volume (solid line).

Figure 12 shows the results of tests for a 1-m^3 extraction vessel with different aspect ratios. Even though the largest ratio resulted in the shortest depressurization time for the same opening, the temperature recovery was best when the aspect ratio was smallest.

This last thing was not expected because of the shorter distance between the vessel wall and its center at larger aspect ratios. Pressure drop seems to be relatively unaffected by aspect ratio through the depressurization, except in the last increase.

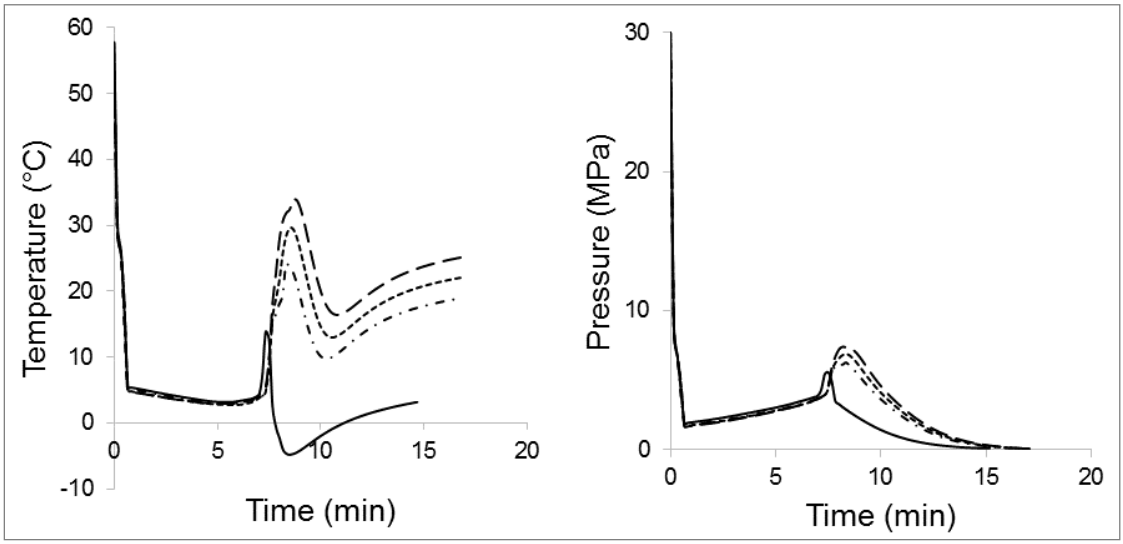

Figure 12. Temperature and pressure changes for depressurizations starting at 60 °C and 30 MPa in a 1 m^3 vessel packed with glass beads with different values for aspect ratio (— — L/D = 4; ------- L/D = 4.5; - · - · - L/D = 5; ——— L/D = 6).

Figure 13 shows the results of tests for a 1-m^3 extraction vessel with different initial pressures. The pressure at which the system reached saturation conditions decreases with higher initial pressures, as observed also by Gebbeken & Eggers (1996). At higher initial pressure, total depressurization time with the same valve opening was higher, as expected. Temperature recovery was better at lower pressures but the minimum temperature reached was not greatly affected by the change in initial pressure.

Results of depressurizations for a 1-m^3 extraction vessel with different initial temperatures are shown in Figure 14 and did not turn out as expected. While depressurizations at 70 °C and 80 °C follow similar patterns, the one starting at 60 °C has a less steep temperature drop and even reaches higher temperatures than the other ones.

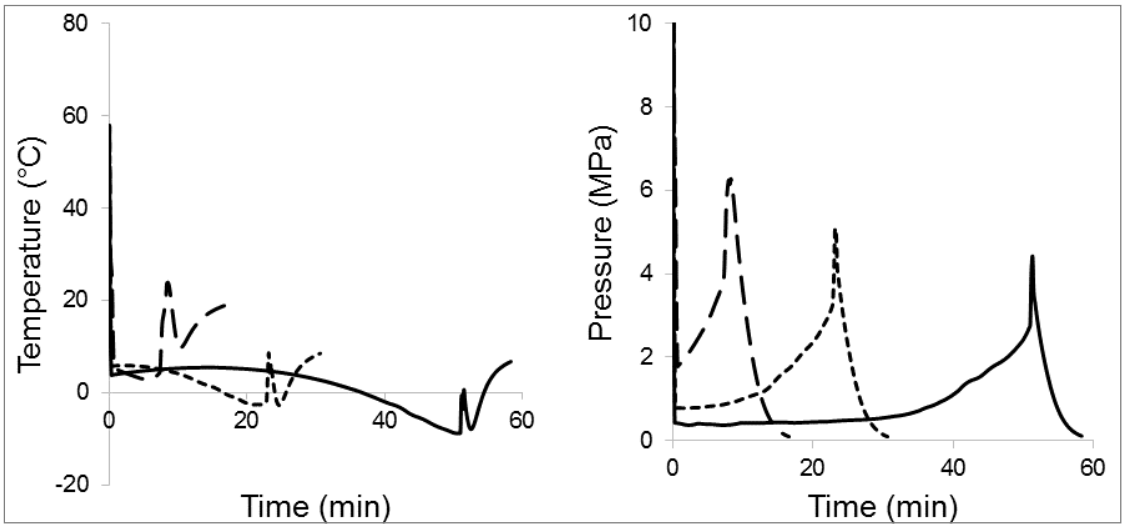

Figure 13. Temperature and pressure changes for depressurizations in a 1 m^3 vessel packed with glass beads starting at 60 °C and with different initial pressures (– – 30 MPa; -------- 50 MPa; ——— 70 MPa).

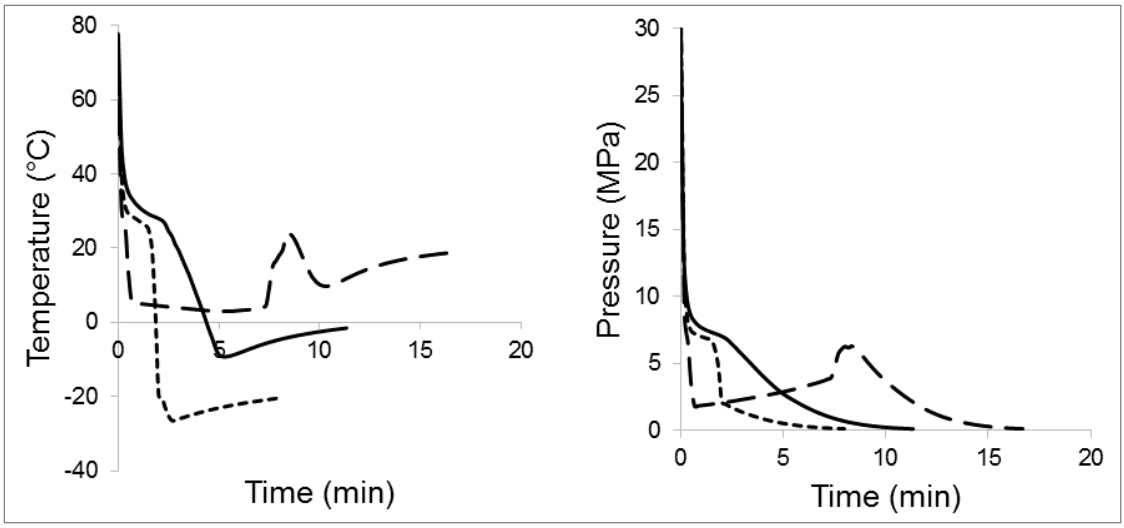

Figure 14. Temperature and pressure changes for depressurizations in a 1 m^3 vessel packed with glass beads starting at 30 MPa and with different initial temperatures (– – 60 °C; -------- 70 °C; ——— 80 °C).

6. DISCUSSION

The developed model was used to simulate depressurizations of extraction vessels as large as 1 m^3, with different vessel geometries, and with different starting temperatures and pressures. Simulated depressurization times went from 4 to 55 minutes, which is in accordance to the reference values reported previously (Fiori, 2010; Quirin & Gerard, 2007). However, some of these times were too short (fast depressurizations), reaching undesirable lower temperatures (less than -10 °C). Simulated times presented in this work are overestimated respect of the times required to depressurize an extraction vessel in an industrial plant at conditions studied where the valve opening is not kept at a constant value, but opened and closed according to what is needed in the operation of the plant. So, our ultimate goal is applying the model to obtain an optimal mass flow of CO_2 leaving the extraction vessel by varying the valve opening in a control loop that incorporates this information.

Temperature and pressure behavior presented the following five stages during the depressurization of extraction vessels of different volumes: i) an abrupt decrease of the variable; then, ii) a *plateau* in which temperature and pressure became stable; iii) another decrease; iv) a rise and fall of temperature (and pressure in larger vessels); and finally, v) a steady rise in temperature, and fall in pressure. This differs from the experimental observations of Richter *et al.* (2015) in a small 1-gallon vessel whose experiments only showed stages (i), (ii), and (v) because their attempts to avoid a gas-liquid transition. This implies that stages (iii) and (iv) are due to gas-liquid transitions phenomena within the extraction vessel during faster depressurization.

The *plateau* reached at stage (ii) could be related to CO_2 evaporation occurring within the vessel, which would be in accordance with the results of Gebbeken & Eggers (1996), who identified phase separation after the initial drop of pressure was over. Local density plays a large role in these changes. In smaller vessels (0.005 and 0.080 m^3), stage (ii) coincides with density increases in the vessel core from 600 to 900 kg m^{-3}, which might

indicate liquid formation in there. Stage (iii) is initiated by the decrease in density from values around 900 to nearly 100 kg m^{-3}, which could mean that all the previously mentioned liquid has been evacuated. In larger vessels, density rapidly decreases from 800 to 50 kg m^{-3}, which explains the longer *plateau* in temperature (stage ii), indicating the onset of evaporation. The increase in pressure in that stage is also explained, as gas takes up more space inside the vessel.

Depressurizations with different initial conditions showed interesting results. In the case of depressurizations of extraction vessels at different starting temperatures, results did not go as expected. The simulated temperature in the depressurization starting at 60 °C differed from the other two. Even more, the final temperature was highest in the depressurization starting at 60 °C, and lowest in the depressurization starting at 70 °C. However, this can be explained by the properties of CO_2 during these depressurizations. In the depressurizations starting at 70 and 80 °C, CO_2 went from a supercritical state (density around 800 kg m^{-3}), to a subcooled liquid state (density around 1100 kg m^{-3}), and then to a superheated gas state (density around 50 kg m^{-3}) during the process. In the case of depressurizations starting at 60 °C, CO_2 transitions almost instantly from a supercritical state to a superheated gas state (density rapidly goes from 800 to 40 kg m^{-3}), which allows it to reach stage (ii) (the *plateau* of temperature) faster than in the other cases. In other words, lower initial temperatures reduce the magnitude of the initial drop by allowing early CO_2 evaporation.

In depressurizations with different starting pressures, the ones with higher starting pressure and the same valve opening area were expected to last longer. However, that seemed to be the only visible effect, as the variations of temperature followed the same patterns in each case. Pressures at the end of stage (i) were lower in depressurizations at higher starting pressures, which was also seen by Gebbeken & Eggers (1996) and attributed to higher initial specific entropy. At higher initial pressures, the pressure needed for CO_2 to transition from a superheated gas state to a subcooled liquid state lowers. This means that it will take longer to reach that pressure inside the vessel and, because of that, temperature reached lower values as initial pressure increased.

In depressurization of extraction vessels with different aspect ratios, it can be seen that, initially, both temperature and pressure seem independent of this factor. This means that even reducing the distance between the wall and the packed bed core does not help compensate the energy loss due to mass flow. However, the temperature at the end of the depressurization is higher when the aspect ratio is smallest. Even though the largest aspect ratio had the shortest depressurization time, the lower final temperature makes further analysis necessary in order to make a recommendation as to which value is best for optimization. If temperature is still close to the minimum temperature allowed, it would not be possible to further open the valve. This means that a smaller aspect ratio could shorten depressurization times by allowing CO_2 to leave the vessel faster.

The simulations described previously were possible after we determined a correlation between *Nu* as a function of *Ra* and *Da* to estimate the convective heat transfer at the vessel wall. The coefficients of this correlation are similar to those proposed by Richter *et al.* (submitted) but predictions were improved by almost 20% when using the parameters obtained through simulation. Confidence intervals support the relevancy of each parameter in the model, even though parameter *b* in Eq. (27) (the exponent of *Da*) is in the order of magnitude of 10^{-2}. This means that *Da* is appropriate to account for the effects of the geometry of the vessel and the properties of the packed bed on convective heat transfer at the vessel wall.

Temperature, pressure, and mass changes during the depressurization experiments carried out by Richter *et al.* (submitted) were simulated. Temperature distributions in Fig. 9 help illustrate the role played by the packed bed on heat transfer. At times where fluid temperature drop is higher, solid temperature drops in order to act as a buffer for the fluid. On the contrary, when temperature is stabilizing, solid temperature is almost homogeneous. These results confirm previous belief (Richter *et al.*, 2015, submitted) that the solid phase acts as a reservoir of energy for the fluid phase and that accuracy in the calculations of physical properties of the solid phase is very relevant for depressurizations.

Initial temperature drop when opening the valve, which was done twice during experiments, is more abrupt in simulated than in experimental results. This could be because the valve opening area is instantly changed in the model but, in reality, opening area takes multiple values in the time it takes for it to change from its initial to its final setting. Also, thermal inertia of the vessel could have been overestimated, which would mean that the heat retained by the vessel walls and by the packed material is not being released into the system as fast as in the model. This difference seems to have a greater effect on pressure drop after the second stage of valve opening than in the first stage. One reason for this could be that pressure was calculated using the mean temperature of the vessel, which has a small deviation at the beginning of the depressurization but not after the second stage.

7. CONCLUSIONS

The objectives of this thesis were achieved successfully. The model here proposed simulated controlled depressurizations reported in previous work reasonably well, and was able to give first insight of depressurization times at different volumes, geometries, and initial conditions.

Exploration tests gave first insight of the effect some operational parameters in the depressurization time. Larger vessels seem to be more affected by gas-liquid transitions than smaller vessels. Initial temperature had an interesting effect on the depressurizations; early evaporation brought on by lower initial temperatures kept temperatures from decreasing below the accepted limit. Aspect ratio (L/D) only affected depressurizations after saturation conditions were met, but further study with varying valve openings is needed to make final suggestions. Experimental results of depressurizations of an extraction vessel at industrial conditions are needed to validate these simulations, and to continue work on simulating depressurizations with varying valve openings.

Phase separation was roughly considered in this model by calculating the properties of CO_2 with a weighted mean using the CO_2 quality as the weight. A final version of this model should consider each phase separately, and include a boundary condition for the point where both phases meet. Also, the correlations used in the model will need to be reassessed once phase separation is completely included to verify that they are suited for the new conditions inside the extraction vessel.

This model can be used to obtain time-to-time values of the valve opening area in order to minimize the process time while keeping temperatures above the acceptable limit. This information could be used as input for a valve process control that constantly modifies the opening of the valve during depressurizations. By optimizing the operational costs of an SFE plant, this technology should become more attractive for investors, and become widely used in the food industry.

NOMENCLATURE

Latin letters

A	Valve opening area (m^2)
Bi	Biot number hLk^{-1} (-)
Da	Darcy number $d_p^2\varepsilon^3\left(150(1-\varepsilon)^2 L^2\right)^{-1}$ (-)
D	Vessel diameter (m)
d_p	Particle diameter (m)
F	Mass flow rate (kg s^{-1})
h	Heat transfer coefficient (W m^{-2} K^{-1})
k	Thermal conductivity (W m^{-1} K^{-1})
l	Packed bed material height (m)
L	Vessel height (m)
m	System fluid mass (kg)
Nu	Nusselt number hLk^{-1} (-)
Pe	Péclet number $RePr$ (-)
Pr	Prandtl number $\nu\alpha^{-1}$ (-)
r	Radial position (m)
R	Vessel internal radius (m)
Ra	Rayleigh number $g\beta\left(T_w-\bar{T}\right)L^3(\nu\alpha)^{-1}$ (-)
Re	Reynold number $ud_p\nu^{-1}$ (-)
T	Temperature (ºC or K)
t	Time (s)
u	Superficial velocity (m s^{-1})
x	Vessel steel wall thickness (m)
z	Axial position (m)

Greek letters

α	Thermal diffusivity (m^2 s^{-1})

β	Younis extinction coefficient (-)
ρ	Density (kg m^{-3})
ε	Porosity
σ	Stefan-Boltzmann constant (W m^{-2} K^{-4})
ν	Dynamic viscosity (m^2 s^{-1})
υ	Speed of sound (m s^{-1})

Subscripts

eff	Effective
f	Fluid
J	Jacket
l	Lid
s	Solid
t	Time
w	Wall

REFERENCES

Bednat, H. H. (1996). *Pressure Vessel Design Handbook* (2nd ed.). Malabar, FL.: Krieger Publ. Co.

Bergman, T. L., Lavine, A. S., Incropera, F. P., & Dewitt, D. P. (2011). *Fundamentals of Heat and Mass Transfer* (7th Editio). Danvers, MA: John Wiley & Sons, Inc.

Brunner, G. (2005). Supercritical fluids: technology and application to food processing. *Journal of Food Engineering*, *67*, 21–33.

del Valle, J. M. (2015). Extraction of natural compounds using supercritical CO_2: Going from the laboratory to the industrial application. *The Journal of Supercritical Fluids*, *96*, 180–199.

Dixon, A. G. (1988). Correlations for wall and particle shape effects on fixed bed. *The Canadian Journal of Chemical Engineering*, *66*, 705–708.

Dixon, A. G., & Cresswell, D. L. (1979). Theoretical prediction of effective heat transfer parameters in packed beds. *AIChE Journal*, *25*(4), 663–676.

Eggers, R., & Green, V. (1990). Pressure discharge from a pressure vessel filled with CO_2. *Journal of Loss Prevention in the Process Industry*, *3*, 59–63.

Fiori, L. (2010). Supercritical extraction of grape seed oil at industrial-scale: Plant and process design, modeling, economic feasibility. *Chemical Engineering and Processing: Process Intensification*, *49*(8), 866–872.

Gamson, B. W., Thodos, G., & Hougen, O. A. (1943). Heat, mass and momentum transfer in the flow of gases through granular solids. *Trans AIChE*, *39*(1), 1–35.

Garcia-Viguera, C., Zafrilla, P., & Tomás-Barberán, F. A. (1998). The use of acetone as an extraction solvent for anthocyanins from strawberry fruit. *Phytochemical Analysis*, *9*(6), 274–277.

Gebbeken, B., & Eggers, R. (1996). Blowdown of carbon dioxide from initially supercritical conditions. *Journal of Loss Prevention in the Process Industries*, *9*, 285–

293.

Gunn, D. J. (1978). Transfer of heat or mass to particles in fixed and fluidised beds. *International Journal of Heat and Mass Transfer*, *21*(4), 467–476.

Herrero, M., Cifuentes, A., & Ibañez, E. (2006). Sub- and supercritical fluid extraction of functional ingredients from different natural sources: Plants, food-by-products, algae and microalgaeA review. *Food Chemistry*, *98*(1), 136–148.

Huang, F., Li, M., Lee, L. L., Starling, K. E., & Chung, F. T. H. (1984). An accurate equation of state for carbon dioxide. *Journal of Chemical Engineering of Japan*, *18*(6), 490–496.

Kunii, D., & Smith, J. M. (1960). Heat transfer characteristics of porous rocks. *AIChE Journal*, *6*(1), 71–78.

Kunii, D., & Suzuki, M. (1967). Particle-to-fluid heat and mass transfer in packed beds of fine particles. *International Journal of Heat and Mass Transfer*, *10*(7), 845–852.

Lemmon, E. W., Huber, M. L., & McLinden, M. O. (2007). *NIST standard reference database 23: mini-reference fluid thermodynamic and transport properties (REFPROP), version 9.0*. Gaithersburg, ML: National Institute of Standards and Technology, Standard Reference Data Program.

Martin, H. (1978). Low peclet number particle-to-fluid heat and mass transfer in packed beds. *Chemical Engineering Science*, *33*(7), 913–919.

Miyauchi, T. (1971). Film coefficients of mass transfer of dilute sphere-packed beds in low flow rate regime. *Journal of Chemical Engineering of Japan*, *4*(3), 238–245.

Mustafa, A., & Turner, C. (2011). Pressurized liquid extraction as a green approach in food and herbal plants extraction: A review. *Analytica Chimica Acta*, *703*(1), 8–18.

Nelson, P. A., & Galloway, T. R. (1975). Particle-to-fluid heat and mass transfer in dense systems of fine particles. *Chemical Engineering Science*, *30*(1), 1–6.

Nield, D. A., & Bejan, A. (2006). *Convection in porous media* (3rd Editio). New York, NY: Springer-Verlag.

Núñez, G. A., & del Valle, J. M. (2014). Supercritical CO_2 oilseed extraction in multi-vessel plants. 2. Effect of number and geometry of extractors on production cost. *The Journal of Supercritical Fluids*, *92*, 324–334.

Núñez, G. A., Gelmi, C. A., & del Valle, J. M. (2011). Simulation of a supercritical carbon dioxide extraction plant with three extraction vessels. *Computers & Chemical Engineering*, *35*, 2687–2695.

Olbrich, W. E., & Potter, O. E. (1972). Mass transfer from the wall in small diameter packed beds. *Chemical Engineering Science*, *27*(9), 1733–1743.

Pfeffer, R., & Happel, J. (1964). An analytical study of heat and mass transfer in multiparticle systems at low Reynolds numbers. *AIChE Journal*, *10*(5), 605–611.

Quirin, K. W., & Gerard, D. (2007). Supercritical fluid extraction (SFE). In *Flavourings. Production, Composition, Applications, Regulations* (2nd. Ed., pp. 44–65). Weinheim, Germany: John Wiley & Sons.

Ranz, W. E. (1952). Friction and transfere coefficients for single particles and packed beds. *Chemical Engineering Progress*, *48*(5), 247–253.

Reverchon, E., & De Marco, I. (2006). Supercritical fluid extraction and fractionation of natural matter. *The Journal of Supercritical Fluids*, *38*(2), 146–166.

Richter, E. A., del Valle, J. M., & Núñez, G. A. (2015). Thermodynamic properties of CO_2 during controlled decompression of supercritical extraction vessels. *The Journal of Supercritical Fluids*, *98*, 102–110.

Richter, E. A., Murias, M. S., & del Valle, J. M. (submitted). Heat transfer and venting rate during controlled decompression of supercritical extraction vessels. *Journal of Supercritical Fluids*.

Schlünder, E. U. (1966). Local heat transfer coefficients in film condensation at high Prandtl numbers. *Chemical Engineering Technology*, *38*, 967–979.

Schlünder, E. U. (1975). *Einführung in die Wärme- und Stoffübertragung*. Wiesbaden: Vieweg+Teubner Verlag.

Schlünder, E. U. (1978). *Chemical Reaction Engineering Reviews—Houston*. (D. Luss & V. W. Weekman, Eds.) (Vol. 72). WASHINGTON, D. C.: American Chemical Society.

Schlünder, E. U., & Tsotsas, E. (1988). *Wärmeübertragung in Festbetten, durchmischten Schüttgütern und Wirbelschichten*. Stuttgart-New York: Thieme Verlag.

Schumann, T. E. W., & Voss, V. (1934). Heat flow through granulated material. *Fuel*, *13*(8), 249–256.

Slimi, K., Ben Nasrallah, S., & Fohr, J. P. (1997). Transient natural convection in a vertical cylinder opened at the extremities and filled with a fluid saturated porous medium : validity of Darcy flow model and thermal boundary layer approximations. *International Journal of Heat and Mass Transfer*, *41*, 1113–1125.

Smallman, R. E., & Ngan, A. H. W. (2007). *Physical metallurgy and advanced materials* (7th Editio). Oxford: Butterworth-Heinemann.

Sørensen, J. P., & Stewart, W. E. (1974). Computation of forced convection in slow flow through ducts and packed beds—I extensions of the graetz problem. *Chemical Engineering Science*, *29*(3), 811–817.

Stanley, S. I. (1998). *Chemical and Engineering Thermodynamics* (3rd Editio). Danvers, MA: John Wiley & Sons, Inc.

Vortmeyer, D., & Schaefer, R. J. (1974). Equivalence of one- and two-phase models for heat transfer processes in packed beds: one dimensional theory. *Chemical Engineering Science*, *29*(2), 485–491.

Wakao, N., & Kaguei, S. (1982). *Heat and Mass transfer in packed beds*. New York, NY: Gordon and Breach.

Wakao, N., Kaguei, S., & Funazkri, T. (1978). Effect of fluid dispersion coefficients on particle-to-fluid heat transfer coefficients in packed beds. *Chemical Engineering Science*, *34*, 325–336.

Winterberg, M., & Tsotsas, E. (2000). Correlations for effective heat transport

coefficients in beds packed with cylindrical particles. *Chemical Engineering Science*, *55*(23), 5937–5943.

Yagi, S., Kunii, D., & Wakao, N. (1960). Studies on axial thermal conductivities in packed beds. *AIChE Journal*, *6*(4), 543–546.

Yagi, S., & Wakao, N. (1959). Heat and mass transfer from wall to fluid in packed beds. *AIChE Journal*, *5*(1), 79–85.

Younis, L. B. (2006). Modelling of hydrogen oxidation within catalytic packed bed reactor. *Journal of the Energy Institute, 79*(4), 222–227.

Zehner, P., & Schlünder, E. U. (1970). On the effective heat conductivity in packed beds with flowing fluid at medium and high temperatures. *Chemical Engineering Technology*, *42*, 933–941.

Zhang, J., Zhu, D., Tian, W., Qiu, S., Su, G., & Zhang, D. (2014). Depressurization study of supercritical fluid blowdown from simple vessel. *Annals of Nuclear Energy*, *66*, 94–103.

APPENDICES

APPENDIX A: CODE USED IN MATLAB TO SIMULATE DEPRESSURIZATION AT DIFFERENT VESSEL VOLUMES AND GEOMETRIES, PACKED BED SUBSTRATE, VALVE OPENING AREA, AND INITIAL PRESSURE AND TEMPERATURE.

```
function [Ti,P,mp,Te]=depressurization(n, m, P0, T0, R, e, h, dp, ks,
rhos, cps, op, shape);

%n = number of nodes for the radial dimension
%m = number of nodes for the axial dimension
%P0 = initial pressure [MPa]
%T0 = initial temperature [°C]
%R = vessel radium [m]
%e = vessel wall thickness [m]
%h = vessel wall height [m]
%dp = particle diameter or equivalent diameter [m]
%ks = substrate termal conductivity [W/mK]
%rhos = substrate density [kg/m3]
%cps = substrate heat capacity [J/kgK]
%op = valve opening area [m2]
%shape = shape of substrate (1 for spheres and 2 for cylinders)

r=linspace(0,R,n);
z=linspace(0,h,m);

%Calculate the bulk and interparticle porosity
dD=dp/2/R;
[por, por_e]=porosity(dD,shape);

%Initial conditions: [T Mass]
V=pi*R^2*h;
M0=V*por*refpropm('D','T',T0,'P',P0*1000,'CO2');
%The matrix por initial values is made up from the substrate
temperatures %(1:n*m), the fluid temperatures (n*m+1:2*n*m), and the
CO2 mass in the %vessel (2*n*m+1)
T0=[(T0+273.15)*ones(2*n*m) M0];

[Ti,Te]=ode23s(@(t,T)
der(t,T,n,m,R,e,h,T0,por,por_e,dp,ks,rhos,cps,op,shape),0:10:5000,T0);

%Border Conditions
for i=1:n
    Te(:,n*m+i)=Te(:,n*m+m+i)-(Te(:,n*m+2*m+i)-Te(:,n*m+m+i))/2;
    Te(:,n*m+(m-1)*n+i)=Te(:,n*m+(m-2)*n+i)-(Te(:,n*m+(m-3)*n+i)-
Te(:,n*m+(m-2)*n+i))/2;
    Te(:,i)=Te(:,m+i)-(Te(:,2*m+i)-Te(:,m+i))/2;
    Te(:,(m-1)*n+i)=Te(:,(m-2)*n+i)-(Te(:,(m-3)*n+i)-Te(:,(m-
2)*n+i))/2;
end
```

```
%Mass flow and pressure calculations
    mp=zeros(length(Ti),1);   %Mass flow vector
    P=mp;                     %Pressure vector
    P(1)=P0;
    for tp=1:length(Ti)-1
        %Mass flow is calculated as the mass difference between two
given
        %times
        mp(tp) = -(Te(tp+1,end)-Te(tp,end))/(Ti(tp+1,end)-Ti(tp,end));
        %Pressure is calculated using the mean temperature and density
at
        %a given time
        P(tp+1) =
pressure(Tprom(Te(tp+1,n*m+1:n*m*2)),Te(tp+1,end)/V/por);
    end
    %
end
```

APPENDIX B: MATLAB FUNCTION USED TO SOLVE THE PARTIAL DIFFERENTIAL EQUATIONS FOR DEPRESSURIZATION

```
function dT = der(t,T,n,m,R,e,h,T0,por,por_e,dp,ks,rhos,cps,op,shape)
V=pi*R^2*h;
dr=R/n;
dz=h/m;
r=linspace(0,R,n);
coef=[0.07774954;-0.0372709;0.3967043];

%CO2 mass in the system
Ms=T(end);

%Mean temperature in the vessel
Tp=Tprom(T(n*m+1:2*n*m));

%Density of the system
D=Ms/(V*por);

%Pressure inside the vessel
P=pressure(Tp,D)*1000;

%Mean thermal conductivity in the vessel (used to calculate particle-
to-%fluid heat transfer coefficient and effective thermal
conductivities)
kf=cond(Tp,P);

%Steel thermal conductivity
temp=[300;400];
k=[13.4;15.2];
ka=interp1(temp,k,273+T0);

%Substrate thermal diffusivity
alphas=ks/(rhos*cps);

%Dimensionless numbers
deltaT=(T(n*m+(m/2-1)*n+1)-T(n*m+(m/2-1)*n+n));
Ra=abs(9.81*b(Tp,P)*deltaT*h^3/(din_vis(Tp,P)*0.0001)^2)*pra(Tp,P);
K=dp^2*por_e^3/150/(1-por_e)^2;
Da=K/h^2;
Nu=coef(1)*Da^coef(2)*Ra^coef(3);
hc=Nu*kf/h;

%Vented mass flow
mp=A*sound(T(n*m+(m-1)*n+1),P)*D;
%Superficial velocity
u=mp/(D*pi*R^2*por);
%Reynolds number
Re=D*u*dp/vis(Tp,P);
%Particle-to-fluid heat transfer coefficient
hfs=(kf/dp)*(2+1.1*pra(Tp,P)^(1/3)*Re^0.6);
%Solid-fluid Exchange area
afs=6*(1-por)/dp;
```

```
%Effective thermal conductivities
kz=kf+ks/((1+16*ks*(1/hfs/dp+0.1/ks)/3)/((1-por)*(2*R/dp)^2))^2;
kr=1+ks*((1+8*kf/hc/R/2)/((1+16*ks*(1/dp/hfs+0.1/ks)/3)/((1-
por)*(2*R/dp)^2)))/kf;

%Partial differential equations
dT=zeros(2*n*m+1,1);
for j=2:m-1
    for i=2:n-1
        %Substrate
        d2Tsdr2=(T((j-1)*n+i+1)-2*T((j-1)*n+i)+T((j-1)*n+i-1))/dr^2;
        dTsdr=(T((j-1)*n+i+1)-T((j-1)*n+i-1))/(2*dr);
        d2Tsdz2=(T((j)*n+i)-2*T((j-1)*n+i)+T((j-2)*n+i))/(dz^2);
        dT((j-
1)*n+i)=alphas*(d2Tsdr2+dTsdr/r(i)+d2Tsdz2+6*hfs*(T(n*m+(j-1)*n+i)-
T((j-1)*n+i))/(ks*dp));
        %Fluid
        kf=cond(T(n*m+(j-1)*n+i),P);
        cp=cap(T(n*m+(j-1)*n+i),P);
        d=refpropm('d','t',T(n*m+(j-1)*n+i),'p',P,'co2');
        d2Tfdr2=(T(n*m+(j-1)*n+i+1)-2*T(n*m+(j-1)*n+i)+T(n*m+(j-1)*n+i-
1))/dr^2;
        dTfdr=(T(n*m+(j-1)*n+i+1)-T(n*m+(j-1)*n+i-1))/(2*dr);
        dTfdz=(T(n*m+(j)*n+i)-T(n*m+(j-2)*n+i))/(2*dz);
        d2Tfdz2=(T(n*m+(j)*n+i)-2*T(n*m+(j-1)*n+i)+T(n*m+(j-
2)*n+i))/(dz^2);
        dT(n*m+(j-1)*n+i)=-
u*dTfdz/por+(2*pi*kr*kf*(r(i)*d2Tfdr2+dTfdr)+pi*kz*kf*2*r(i)*d2Tfdz2-
hfs*afs*2*pi*r(i)*(T(n*m+(j-1)*n+i)-T((j-1)*n+i))-mp*ent(T(n*m+(j-
1)*n+i),P)/R/h)/(por*d*cp*pi*2*r(i));
    end
    %Border conditions
    %Fluid at the center
    dT(n*m+(j-1)*n+1)=(4*dT(n*m+(j-1)*n+2)-dT(n*m+(j-1)*n+3))/3;
    %Fluid at the wall
    dT(n*m+(j-1)*n+n)=dT(n*m+(j-1)*n+1)*hc/(hc+ka/e);
end

%Border conditions
for j=1:m
    %Substrate at the center
    dT((j-1)*n+1)=(4*dT((j-1)*n+2)-dT((j-1)*n+3))/3;
    %Substrate at the wall
    dT((j-1)*n+n)=(4*dT((j-1)*n+n-1)-dT((j-1)*n+n-2)+2*dr*ka*(Tch-T((j-
1)*n+n))/e/ks)/3;
end

for i=2:n-1
    %Substrate at lower lid
    dT(i)=(4*dT(n+i)-dT(2*n+i))/(3);
    %Substrate at upper lid
    dT((m-1)*n+i)=(4*dT((m-2)*n+i)-dT((m-3)*n+i))/(3);
end
```

```
for i=1:n
    %Fluid at lower lid
    dT(n*m+i)=dT(n*m+(m/2-1)*n+1)*hc/(hc+ka/e/1.4);
    %Fluid at lower lid
    dT(n*m+(m-1)*n+i)=dT(n*m+(m/2-1)*n+1)*hc/(hc+ka/e/1.4);
end
%Mass flow
dT(2*n*m+1)=-mp;
end
```

APPENDIX C: MATLAB FUNCTION USED TO CALCULATE VESSEL PRESSURE

```
function p=pressure(T,D)
%Calculates pressure using Huang et al. (1984) correlation
Tcrit=refpropm('T','C',0,' ',0,'co2');
Dcrit=refpropm('D','C',0,' ',0,'co2')/0.044;

Tp=T/Tcrit;
Dp=D/0.044/Dcrit;
dT=1-Tp;
dD=1-1/Dp;

b=ones(7,1);
c=ones(27,1);

c(1)=0.376194;
c(2)=0.118836;
c(3)=-3.04379;
c(4)=2.27453;
c(5)=-1.23863;
c(6)=0.250442;
c(7)=-0.11535;
c(8)=0.675104;
c(9)=0.198861;
c(10)=0.216124;
c(11)=-0.583148;
c(12)=0.0119747;
c(13)=0.0537278;
c(14)=0.0265216;
c(15)=-2.79498;
c(16)=5.62393;
c(17)=-2.93831;
c(18)=0.988759;
c(19)=-3.04711;
c(20)=2.32316;
c(21)=1.07379;
c(22)=-6.00E-05;
c(23)=8.85E-05;
c(24)=3.16E-03;
c(25)=10.00;
c(26)=50.00;
c(27)=80000;

b(1)=c(1)+c(2)/Tp+c(3)/Tp^2+c(4)/Tp^3+c(5)/Tp^4+c(6)/Tp^5;
b(2)=c(7)+c(8)/Tp+c(9)/Tp^2;
b(3)=c(10)+c(11)/Tp;
b(4)=c(12)+c(13)/Tp;
b(5)=c(14)/Tp;
b(6)=c(15)/Tp^3+c(16)/Tp^4+c(17)/Tp^5;
b(7)=c(18)/Tp^3+c(19)/Tp^4+c(20)/Tp^5;
```

```
Z=1+b(1)*Dp+b(2)*Dp^2+b(3)*Dp^3+b(4)*Dp^4+b(5)*Dp^5+b(6)*Dp^2*exp(-
c(21)*Dp^2)+b(7)*Dp^4*exp(-c(21)*Dp^2)+c(22)*Dp*exp(-
c(27)*dT^2)+c(23)*dD/Dp*exp(-c(25)*dD^2-c(27)*dT^2)+c(24)*dD/Dp*exp(-
c(26)*dD^2-c(27)*dT^2);

p=(Z*D/0.044*T*8.314)*0.000001;

if p <0
    p=0.001;
end
end
```

APPENDIX D: MATLAB FUNCTION USED TO CALCULATE BULK POROSITY

```
function [por,por_e]=porosity(dD,shape)
%Calculates bulk porosity for spheres or cylinders
por=0;
por_e=0;
if shape == 1
    if dD <= 0.5
        por=0.4+0.05*dD+0.412*dD^2;
    elseif dD > 0.5 && dD <= 0.536
        por=0.528+2.464*(dD-0.5);
    elseif dD > 0.536
        por=1-0.667*dD^3*(2*dD-1)^(-0.5);
    end
    por_e=por;
elseif shape == 2
    if dD <= 0.6
        por=0.36+0.1*dD+0.7*dD^2;
    elseif dD > 0.6 && dD <= 0.7
        por=0.677-9*(dD-0.625)^2;
    elseif dD > 0.7
        por=1-0.763*dD^2;
    end
    por_e=(por-0.25)/0.75;
end
end
```

APPENDIX E: MATLAB FUNCTIONS USED TO CALCULATE PHYSICAL PROPERTIES OF CO_2

```
function cP=cap(T,D)
%Calculates mean heat capacity when phase separation occurs
if T<304.13,
    quality=refpropm('Q','T',T,'p',D,'CO2');
    if quality<=1 && quality>=0,
        cP=(quality*refpropm('C','T',T,'Q',1,'CO2')+(1-
quality)*refpropm('C','T',T,'Q',0,'CO2'));
    else
        cP=refpropm('c','T',T,'p',D,'CO2');
    end
else
    cP=refpropm('c','T',T,'p',D,'CO2');
end
end

function k=cond(T,D)
%Calculates mean thermal conductivity when phase separation occurs
if T<304.13,
    quality=refpropm('Q','T',T,'p',D,'CO2');
    if quality<=1 && quality>=0,
        k=(quality*refpropm('L','T',T,'Q',1,'CO2')+(1-
quality)*refpropm('L','T',T,'Q',0,'CO2'));
    else
        k=refpropm('L','T',T,'p',D,'CO2');
    end
else
    k=refpropm('L','T',T,'p',D,'CO2');
end
end

function h=ent(T,D)
%Calculates mean enthalpy when phase separation occurs
if T<304.13,
    quality=refpropm('Q','T',T,'p',D,'CO2');
    if quality<=1 && quality>=0,
        h=(quality*refpropm('h','T',T,'Q',1,'CO2')+(1-
quality)*refpropm('h','T',T,'Q',0,'CO2'));
    else
        h=refpropm('h','T',T,'p',D,'CO2');
    end
else
    h=refpropm('h','T',T,'p',D,'CO2');
end
end

function p=pra(T,D)
%Calculates mean Prandtl number when phase separation occurs
if T<304.13,
    quality=refpropm('Q','T',T,'p',D,'CO2');
```

```
    if quality<=1 && quality>=0,
        p=(quality*refpropm('^','T',T,'Q',1,'CO2')+(1-
quality)*refpropm('^','T',T,'Q',0,'CO2'));
    else
        p=refpropm('^','T',T,'p',D,'CO2');
    end
else
    p=refpropm('^','T',T,'p',D,'CO2');
end
end

function mu=vis(T,D)
%Calculates mean dynamic viscosiy when phase separation occurs
if T<304.13,
    quality=refpropm('Q','T',T,'p',D,'CO2');
    if quality<=1 && quality>=0,
        mu=(quality*refpropm('v','T',T,'Q',1,'CO2')+(1-
quality)*refpropm('v','T',T,'Q',0,'CO2'));
    else
        mu=refpropm('v','T',T,'p',D,'CO2');
    end
else
    mu=refpropm('v','T',T,'p',D,'CO2');
end
end

function vel=sound(T,D)
%Calculates mean speed of sound when phase separation occurs
if T<304.13,
    quality=refpropm('Q','T',T,'p',D,'CO2');
    if quality<=1 && quality>=0,
        vel=(quality*refpropm('a','T',T,'Q',1,'CO2')+(1-
quality)*refpropm('a','T',T,'Q',0,'CO2'));
    else
        vel=refpropm('a','T',T,'p',D,'CO2');
    end
else
    vel=refpropm('a','T',T,'p',D,'CO2');
end
end

function beta=b(T,D)
%Calculates mean volumetric expansivity when phase separation occurs
if T<304.13,
    quality=refpropm('Q','T',T,'P',D,'CO2');
    if quality<=1 && quality>=0,
        beta=(quality*refpropm('b','T',T,'Q',1,'CO2')+(1-
quality)*refpropm('b','T',T,'Q',0,'CO2'));
    else
        beta=refpropm('b','T',T,'p',D,'CO2');
    end
else
    beta=refpropm('b','T',T,'p',D,'CO2');
end
```

```
end

function v=din_vis(T,D)
%Calculates mean kinematic viscosity when phase separation occurs
if T<304.13,
    quality=refpropm('Q','T',T,'P',D,'CO2');
    if quality<=1 && quality>=0,
        v=(quality*refpropm('$','T',T,'Q',1,'CO2')+(1-
quality)*refpropm('$','T',T,'Q',0,'CO2'));
    else
        v=refpropm('$','T',T,'P',D,'CO2');
    end
else
    v=refpropm('$','T',T,'P',D,'CO2');
end
end

function T=Tprom(vT)
%Calculates mean mean temperature for a given vector
suma=0;
L=length(vT(1,:));
L2=length(vT(:,1));
for i=1:L
    for j=1:L2
        suma=suma+vT(j,i);
    end
end
T=s/(L*L2);
end
```

APPENDIX F: GEOMETRY OF THE VESSELS USED IN EXPLORATION TESTS

Table 5. Geometry of the vessels used in exploration tests.

Vessel volume (L)	Aspect ratio (L/D)	Initial temperature (°C)	Initial pressure (MPa)	Vessel diameter (m)	Vessel height (m)	Thickness of the wall (m)	Thickness of the lid (m)
5	5.0	60	30	0.108	0.54	0.023	0.019
80	5.0	60	30	0.273	1.37	0.059	0.049
250	5.0	60	30	0.399	2.00	0.086	0.071
500	5.0	60	30	0.503	2.52	0.109	0.089
1000	4.0	60	30	0.683	2.73	0.147	0.121
1000	4.5	60	30	0.656	2.95	0.142	0.117
1000	5.0	60	30	0.634	3.17	0.137	0.113
1000	6.0	60	30	0.596	3.58	0.129	0.106
1000	5.0	60	50	0.634	3.17	0.276	0.192
1000	5.0	60	70	0.634	3.17	0.488	0.276
1000	5.0	70	30	0.634	3.17	0.137	0.113
1000	5.0	80	30	0.634	3.17	0.137	0.113

APPENDIX G: EVOLUTION OF DENSITY THROUGHOUT EXPLORATION TESTS

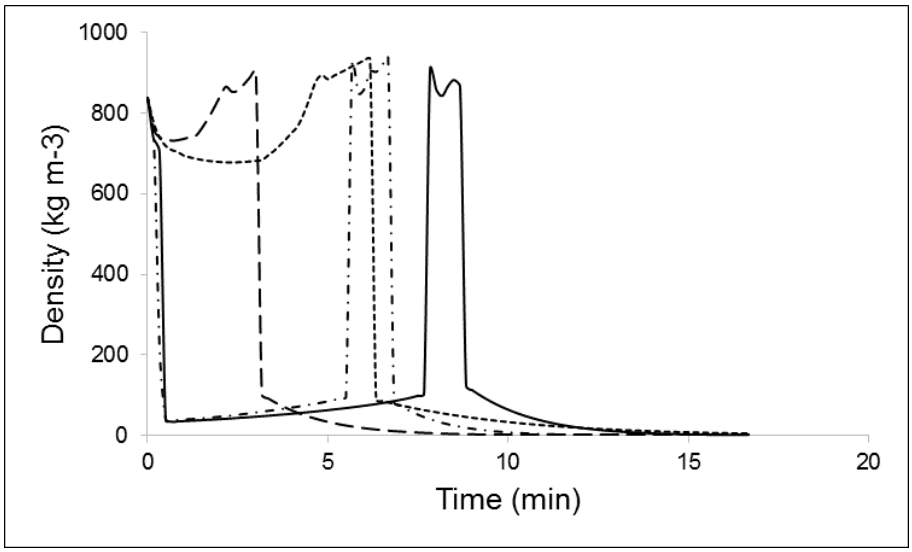

Figure 15. Evolution of density for depressurizations starting at 60 °C and 30 MPa with different vessel volumes (— — V = 0.005 m^3; -------- V = 0.08 m^3; - · - · - V = 0.25 m^3; ——— V = 1 m^3) packed with glass beads.

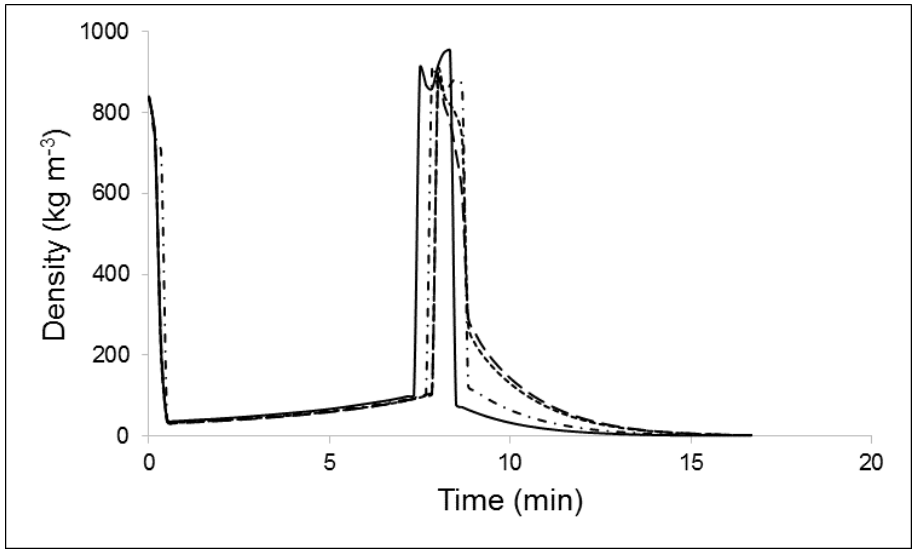

Figure 16. Evolution of density for depressurizations depressurizations starting at 60 °C and 30 MPa in a 1 m^3 vessel packed with glass beads with different values for aspect ratio (— — L/D = 4; -------- L/D = 4.5; - · - · - L/D = 5; ——— L/D = 6).

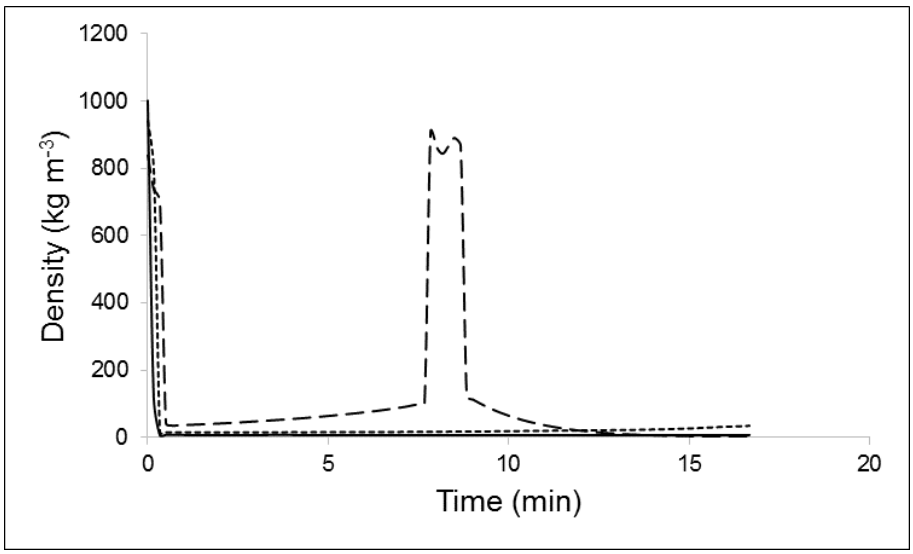

Figure 17. Evolution of density for depressurizations in a 1 m^3 vessel packed with glass beads starting at 60 °C and with different initial pressures (— — 30 MPa; ------- 50 MPa; ——— 70 MPa).

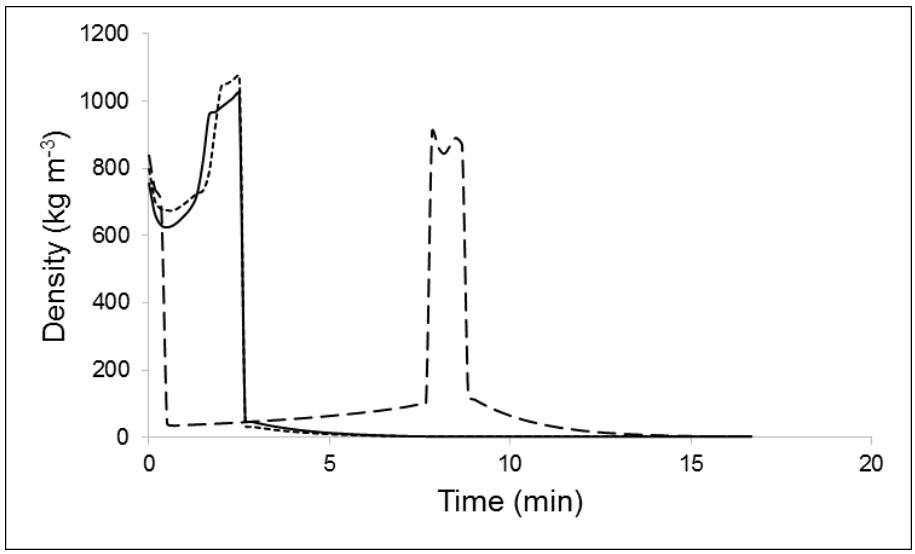

Figure 18. Evolution of density for depressurizations in a 1 m^3 vessel packed with glass beads starting at 30 MPa and with different initial temperatures (— — 60 °C; ------- 70 °C; ——— 80 °C).